Geol. Mag. **143** (*3*), *2006, pp. 343–365.* © *2006 Cambridge University Press*
doi:10.1017/S0016756806001749 *Printed in the United Kingdom*

Environmental control on granular clinoforms of ancient carbonate shelves

A. QUIQUEREZ*‡ &G. DROMART§

*UMR CNRS 5561 Biogéosciences, UFR des Sciences de la Terre, Université de Bourgogne, 6 bd Gabriel, 21000 Dijon, France
§UMR CNRS 5570, Ecole Normale Supérieure de Lyon, Laboratoire de Sciences de la Terre, 46 allée d'Italie, 69634 Lyon Cedex 07, France

(*Received* 27 July 2004; *revised version received* 22 August 2005; *accepted* 7 October 2005)

Abstract – The purpose of this paper is to document the influence of depositional environments on shallow-water, low-relief clinoforms from the description of five ancient carbonate platforms: the Neoproterozoic (Namibia), Middle Jurassic (France), Lower Cretaceous (France), Upper Cretaceous (Oman) and Miocene (Turkey). These examples have been investigated on the basis of field observations. The clinoforms are described with reference to geometric and compositional attributes: declivity, shape, height, sedimentary structures, sediment fabric and components. The results show great variability in stratal geometry, declivity and facies distribution: (1) depositional profiles vary from exponential, to sigmoidal, to oblique; (2) maximal slope angles range from 3 to 25°, most of them being grouped between 10 and 18°; (3) facies differentiation identified from lateral facies successions along beds, and vertical facies successions through beds, is pronounced to subtle. This study documents linkages between depositional environments and clinoform attributes. Proximal/shallow clinoforms display round-edged exponential profiles. Sediment deposition has resulted from unidirectional currents in the upper convex section, and storm-generated oscillatory currents in the lower concave part. The sediment fabric changes gradually along this type of clinoform. There is little vertical facies differentiation through these clinobeds which have formed from a continuous amalgamation of deposits. By contrast, distal clinoforms (shelf break, distally steepened ramp settings) yield a much broader spectrum of profiles and are generally shorter and steeper. Sedimentary structures in gravel-sized deposits of the upper slope indicate pure traction by unidirectional currents. Conversely, marks of oscillatory flows (undular, wavy top bounding surfaces of clinobeds) are common in the lower slope. Intercalation of massive, fine-grained deposits suggests offshore transport of carbonate mud by suspension. Each distal clinobed represents a single flow event. Accordingly, facies differentiation is weak laterally but may be pronounced through the clinobeds. Our study suggests that low-relief forms of proximal/shallow environments, which contain coarse-grained and photo-independently produced debris, record hydrodynamic equilibrium profiles, whereas the higher-relief forms of this setting rather reflect a high differential production rate of carbonate sediment with water depth. The carbonate sediment of the distal clinobeds mainly derives from skeletal production by oligophotic and photo-independent biota of the middle shelf/ramp and upper portion of the clinoforms. The contribution by *in situ* skeletal biota only becomes significant on the lower slope, indicating that the distal, submerged slopes of carbonate platforms are not organically but hydrodynamically generated. Our compilation shows that the slope angles of shallow marine, low-relief clinoforms do not simply correlate to the sediment grain size and fabric, in contrast to what has been documented for the high, linear slope profiles. This difference stems from the depositional settings, namely the involved transport mechanisms. Low-relief clinoform accretion seems to be dominantly influenced by wave-induced sediment transport, in contrast to linear flanks of high-relief clinoforms that build to the angle of repose, and for which gravity is the primary transport process.

Keywords: carbonate platforms, clinoform, geometry, depositional facies, depositional environment.

1. Introduction

Clinoforms are sloping depositional surfaces that form progradation patterns. Mitchum, Vail & Sangree (1977) suggested that clinoform shapes, at the seismic scale, record depositional conditions, specifically variations in accommodation and sediment supply. Bosellini (1984) brought carbonate clinoforms to the forefront by documenting high-relief progradation features in the Dolomites in northern Italy. To date, much work has been dedicated to the study of the stacking pattern of carbonate clinoforms (Pomar, 1991; Jacquin *et al.* 1991; Sonnenfeld & Cross, 1993; K. McDonough, unpub. Ph.D. thesis, Colorado Sch. Mines, 1997) and numerous studies have dealt with the geometry and facies characterization of clinoforms (Mullins *et al.* 1983;

‡Author for correspondence: Amelie.Quiquerez@u-bourgogne.fr

Corso, Austin & Buffler, 1989; Kenter & Campbell, 1991; Blendinger, 1994; Harris, 1994; Bahamonde, Colmenero & Vera, 1997). The major motivation of all these studies has been to gain information about sediment composition and rock properties along depositional slopes that are detectable in seismic data. Comparatively limited attention has been paid to the depositional processes involved in clinoform accretion.

On the basis of observation of seismic profiles off large-scale modern shelves (Mullins *et al.* 1983; Kenter, 1990; Eberli *et al.* 1993; Adams & Schlager, 2000), current facies models for submarine slopes predict the dominance of debris and grain-flows. The large range of slope angles observed for carbonate clinoforms in the rock record has accordingly been interpreted as reflecting equilibrium profiles in which the slope angle corresponds to the angle of repose of grains (Kenter, 1990; Adams & Schlager, 2001), suggesting that avalanching is the ultimate transport mechanism operating on submarine carbonate slopes. However, it should be noted that the systems in which the slope angle is directly correlated to grain size are restricted to high (> 100 m) linear slope profiles. These systems, apparently built to the angle of repose, include flanks of isolated carbonate platforms (Keim & Schlager, 1999), reef talus (Bahamonde *et al.* 2004), and large-scale platform-to-slope settings (Adams *et al.* 2002). Our work aims to explore another spectrum of carbonate slope profiles, particularly by investigating low-relief features from shallow marine environments, that is, the domain of sediment transport by waves.

In this paper, we describe an assortment of ancient slopes that are well exposed in outcrop. Five original examples come from our field observations and one has been incorporated from the literature. This set of slope profiles thus covers a large range of depositional systems, including the shoreface, ramp crest, outer ramp distal slope and shelf break (Read, 1985). The present study is not concerned with fore-reef slopes and flanks of isolated platforms. Descriptions of each example are organized according to the position they occupied on their respective depositional platforms. A general synthesis for stratal geometries and facies attributes (declivity, shape, relief, bedding and related sedimentary structures, sediment fabric and constituents) of all clinoforms described is presented. Finally, the influence of the depositional setting on geometric and faciological characteristics of clinoforms is discussed through a comparison between proximal/shallow and distal environments, respectively.

The purpose of the study is to document how low-relief carbonate slope profiles and their facies distributions are influenced by the environment in which they formed, namely hydrodynamic sediment transport and carbonate-producing biota. Our general objective in studying the clinoforms of carbonate platforms is two-fold: (1) to add information from field analogues about sediment composition to improve the empirical prediction of facies distribution along depositional slopes seen on seismic profiles; (2) to provide forward stratigraphic models with process-based laws for properly simulating sediment dispersal, particularly for fine-tuning the combination of fluid-flow and diffusive approaches (Quiquerez *et al.* 2004).

2. Material and methods

Five cases of ancient shallow-water, low-relief (5–100 m) carbonate clinoforms were selected. They include the Neoproterozoic (Namibia), the Middle Jurassic (France), the Lower Cretaceous (France), the Upper Cretaceous (Oman) and the Miocene (Turkey). The practical criterion for selection is the possibility in the field of continuous observation of clinobeds and bounding surfaces (Fig. 1a). Fundamentally, these examples have been chosen to encompass distinct geodynamic settings (e.g. foreland basin, passive margin), palaeogeographic conditions (open shelves, ramps) and distinct carbonate ecosystems (e.g. eutrophic to oligotrophic skeletal biota), so that we can evaluate the influence of depositional environments on clinoform features. The data come from field studies (rock samples, local measurements and observations) and include line-drawing from photomosaics. The selected sites show no to minimal post-depositional tectonic disturbance at the clinoform scale, thereby leaving depositional profiles unmodified. Clinoform geometries (shape, slope, height and lateral extent) and clinofacies (sedimentary structure, original fabric and components) can be considered as unaltered.

Figure 1a illustrates the terminology used to characterize geometric attributes of clinoforms, following Rich (1951). The suffix '-form' refers to the geomorphic unit, that is, the clinoform. The suffix '-them' refers to the rock unit. Therefore, clinothems are defined as clinobeds bounded by widespread hiatal surfaces (Fig. 1a). From the top to the base, an ideal clinoform profile should successively cross the flat-topped units composed of flat-laminated beds, then the upper slope units, the middle slope and finally the toe-of-slope units.

Clinoform morphologies have been described after the seismic classification proposed by Mitchum, Vail & Sangree (1977) and after the equivalent mathematical description of Adams & Schlager (2000), but adapted to our shallow water clinoforms (Fig. 1b). We have distinguished on this basis three clinoform shapes: (1) the straight morphology, associated with linear clinoforms (parallel or not) with angular foresets, and defined by one or two linear equations, referred to here as 'oblique', (2) the concave morphology characterized by a sharp-edged exponential profile, and referred to as 'exponential', (3) the sigmoidal shape, characterized by a round-edged profile, and referred to as 'sigmoidal'. Within the sigmoidal shapes, we have identified two specific profiles. We have defined the symmetrical sigmoidal shape, or its equivalent mathematical gaussian profile, characterized by an

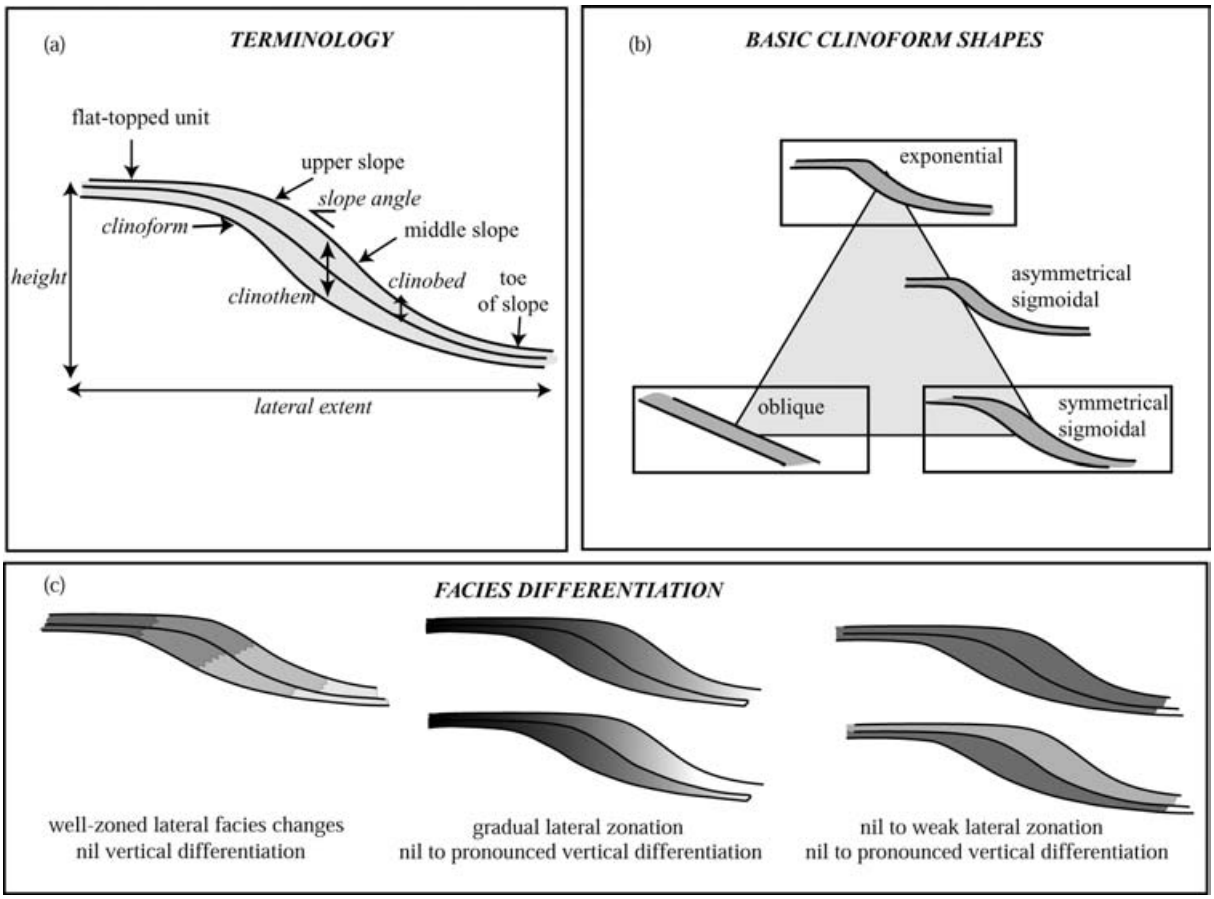

Figure 1. Terminology and definitions used in this paper. See text for explanation.

upper convex part whose lateral extension is identical to the lower concave section, here referred to as 'symmetrical sigmoidal'. We have defined a new shape, composed of a narrow upper convex part, and a much broader lower concave section. This shape is intermediate between symmetrical sigmoidal and exponential geometries, and referred to as 'asymmetrical sigmoidal'.

In the field, clinoform slope angles were repeatedly measured and corrected for structural dip, and bounding surfaces were walked out. For exponential and asymmetrical clinoforms, we measured slope angles at the upper one-third (by height) of the slope. For sigmoidal profiles, we measured slope angle at the inflexion point. Clinoform height has been evaluated from photomosaics and corrected for perspective effects if necessary. Height corresponds to the maximum vertical relief of an individual clinoform between two horizontal surfaces: the upper limit where the clinoform merges and the toe-of-slope. Estimates correspond to minimum values if updip truncation of strata occurs.

Facies are defined with respect to sedimentary structures (physical and biogenic structures, also omission and erosion surfaces), sediment fabric (mud content and grain size distribution) and grain composition. In our study, wherever possible, individual clinoforms were walked out to describe lateral facies differentiation. In the field, rocks were regularly sampled along clinoforms to check sediment fabric and sediment composition evolution through inspection of thin-sections. Additional rock samples were taken where facies change, for example, where sedimentary structures are modified. Therefore, we identify and classify lateral facies differentiation by combining micro- and macro-observations. Lateral facies differentiations are uniform when no changes in sedimentary structures, sediment fabrics and biota are observed. Lateral facies differentiations are well-zoned if sedimentary structures, sediment fabrics and biota all evolve in stages along clinobeds, yielding well-defined facies belts (Fig. 1c). Between these two end-members, gradual lateral facies differentiation can be found where distinctive, variably contrasted facies are recognizable, but no precise contact can be located in the field. We also tried to check vertical facies differentiation following our lateral facies differentiation methodology. Vertical facies differentiation is defined as vertical facies evolution from one bed to another, or one group of beds to another, for the same location on the clinoform slope. Vertical facies differentiation is significant if at least one of the three descriptive facies components (structure, sediment fabric, and biota) sharply changes through beds, or a group of beds, at the same location on the clinoform slope. The various types of lateral and vertical facies evolution encountered in our study are described in Fig. 1c.

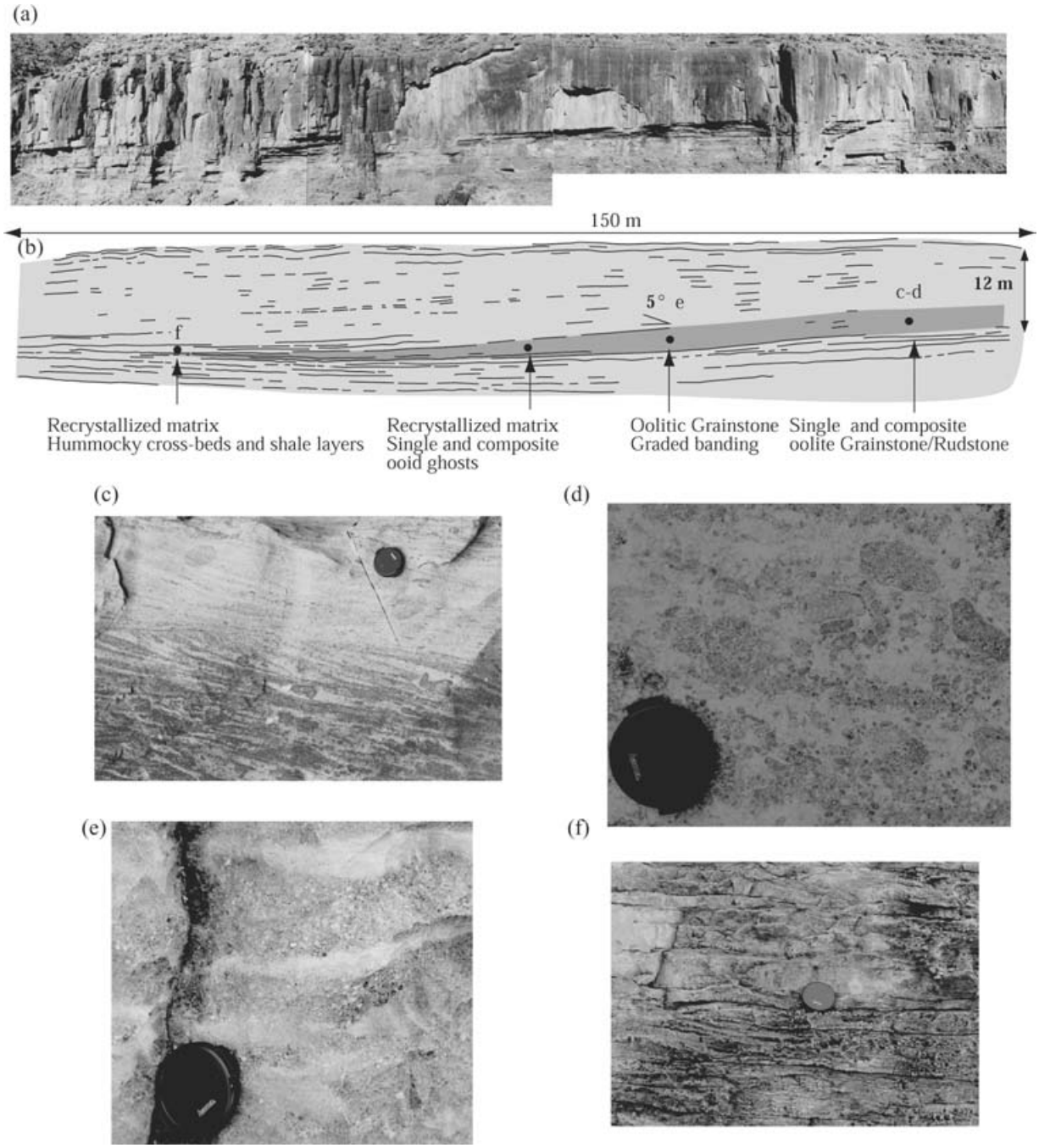

Figure 2. (a) Photograph and (b) line drawing of low-angle, asymmetrical sigmoidal (round-edged exponential) clinoforms in Zebra River Area, Namibia (terminal Proterozoic). Outcrop close-up of depositional facies along a single clinoform. (c) Trough cross-beds in the upper slope, composed of (d) gravel-sized, composite oolites. Storm-generated structures in the middle slope such as (e) sub-horizontal graded banding and (f) amalgamated hummocky cross-beds. Diameter of lens cap is 5 cm.

3. Case histories

Here we describe geometries and facies in terms of lateral facies differentiation and vertical facies differentiation for proximal/shallow versus distal clinoforms. Interpretation of clinoform environments, that is, distinction between proximal and distal clinoforms, is based on already available and independent evidence, including regional stratigraphic correlations and observed depositional facies to confirm depositional environments. Facies are described in detail in Table 1 and specifically in Table 2 for the lower wedge of the Miocene (Turkey).

3.a. Proximal/shallow clinoforms

3.a.1. Terminal Proterozoic of southwestern Namibia (Fig. 2)

The study site is located south of the Naukluft Nappe Complex in the northern Nama Basin in southwestern Namibia (Zebra River Area; 24°35′ S/16°18′ E). The investigated terminal Proterozoic strata belong to the

lower Nama Group (Kuibis Subgroup, Zaris Formation, Hoogland Member), and have been dated at 548.8 ± 1 Ma (U–Pb zircon age) (Grotzinger *et al.* 1995; Saylor *et al*. 1998). Much of the Nama Group was deposited in a foreland basin that developed during convergence along the bordering Damara and Gariep compressional belts (Germs, 1983). The 300 m thick Hoogland Member accumulated as a carbonate ramp (O. Smith, unpub. M.S. thesis, Massachusetts Inst. Tech., 1999).

Gently dipping asymmetrical sigmoidal clinoforms can be seen on both sides of a number of canyons cutting into the carbonate Hoogland Member (Fig. 2a). Massive packages, several metres thick, of amalgamated carbonate beds pinch out over a distance of around one hundred metres, and pass laterally into heterolithic bundles composed of shale, and decimetre-thick carbonate interbeds (Fig. 2a, b). Individual clinoforms exhibit about 5 m of relief from top units to toe-of-slope and extend 150 m laterally. Slope profiles are inclined up to about 5°.

Observations down individual carbonate clinoforms reveal a well-zoned profile with evidence of combined flows in the upper slope (graded composite beds) and profuse structures of oscillatory and unidirectional currents in the lower–middle slope (Fig. 2a–f; Table 1). The average sediment grain size decreases downslope, coincident with limited transfer of coarser ooids and composite ooids from flat-topped units to middle slope and no further. The facies assemblages along the profile are not those of a typical shoreface environment, since wave-ripples and ravinement surfaces are not observed (Table 1). Instead they are interpreted as representing the accretionary margin of an ooid shoal, that is, a ramp crest, subjected to episodic strong flow (recurrent storm events). It was not possible to study vertical facies differentiation at this site.

3.a.2. Middle Jurassic Burgundy platform (Roche de Vergisson) (Fig. 3)

The Burgundy area represents the southeastern margin of the flexural, intracratonic Mesozoic Paris Basin (Robin *et al.* 2000). Major faults crossed the basin at that time and separated high and low topographic zones (Guillocheau *et al.* 2000). The Burgundy–Jura block is one of the major substratum highs over which a subtropical carbonate platform developed during the early Middle Jurassic (Aalenian–Bajocian) (Rousselle & Dromart, 1996; Durlet & Thierry, 2000). The Roche de Vergisson is a topographic spur localized west of the city of Mâcon in South Burgundy. The exposure corresponds to a lithological unit regionally referred to as 'Calcaires à entroques' Formation and is late Early Bajocian in age (J. M. Filak, unpub. Mémoire de DEA, Univ. Bourgogne, 1995; Durlet & Thierry, 2000).

The cliff exposes two stacked, massive, multi-metre thick carbonate wedges that pinch out over a distance of about a hundred metres (Fig. 3a, b). Each wedge exhibits oblique clinoforms and about 5 m of relief. The top-bounding surface of the upper wedge shows a regular gentle dip of about 3°, relative to the basal surface (Fig. 3b). Wedges are separated by red-coloured, burrowed shales. The upper part of the lowermost wedge shows well-marked storm-related ridges and furrows (Fig. 3d). These deep furrows are filled with self-supported, gravel-sized echinoderm and coral debris (Fig. 3e–g). Downlapping clinobeds (locally, slope angle of 6° and differential progradation direction of 50°) are conspicuous in the basal part of the upper wedge (Fig. 3c). Each clinobed in this upper wedge is composed of a crinoidal-dominated grainstone with a variable admixture of bivalve and coral debris, and peloids (Fig. 3e–g). Observations along individual clinoforms reveal a grain-size decrease from gravel-sand to medium coarse-sand size with better sorting towards toe-of-slope, suggesting that lateral facies differentiation occurs gradually along the slope (Table 1). Identical facies assemblages have been observed vertically between clinobeds. The facies assemblage along the profile of the Roche de Vergisson in the Burgundy area is indicative of a proximal shelf setting.

3.a.3. Lower Cretaceous of the Vercors Plateau, southeastern France (La Montagnette) (Fig. 4)

A Lower Cretaceous carbonate platform is located at the southern edge of the Vercors Plateau flanking the Vocontian Basin. Early Cretaceous extensional tectonics related to the opening of the Bay of Biscay (North Atlantic) created a complex rugged topography across the Vocontian Basin (Graciansky & Lemoine, 1988). The Barremian carbonate platforms grew on topographically high blocks in a subtropical environment, on storm-influenced open shelves (Masse *et al.* 1993). The studied strata belonging to the Barremian Glandasse Bioclastic Limestone Formation (Arnaud, 1981) are exposed in the Montagnette Valley (Vallon de Combeau) (Fig. 4).

The Montagnette cliff exposes spectacular clinoforms prograding S/SW over a distance of about one kilometre (Fig. 4a). Three progradation wedges are distinguished on the basis of their basinwards progradation direction (Fig. 4b). Clinoforms from the middle wedge prograde parallel to exposure, whereas the progradation direction of the lower and upper wedges is oblique to the cliff (Fig. 4a, b).

Clinoforms display asymmetrical sigmoidal to symmetrical sigmoidal shapes, most of them being asymmetrical sigmoidal. Dip angles range from 14 to 21° with an average basinwards dip of about 15° relative to a Lower Cretaceous horizontal base level. Height of individual clinoforms is about 50 m. Lateral clinoform extensions range from 200 m to 800 m.

Table 1. Detailed facies description, including sedimentary structures, sediment fabrics and components along clinoforms for each case studied

Age/location	Flat-topped unit	Upper slope	Middle slope	Toe-of-slope
Langhian, Miocene, Cenozoic				
Ermenek, Taurus, Turkey *Upper wedge*	• well-sorted packstone milliolids and alveolinids benthic foraminifers no sedimentary structures	• poorly-sorted packstone debris of corals, red algae echinoderms and benthic foraminifers miliolids, nubecularids, operculinids	• wackestone red-algal filaments, Amphistegina fragments of thick-shelled bivalves no sedimentary structures	• poorly-sorted packstone benthic foraminifers (Heterostegina) and planktonic foraminifers no sedimentary structures
Turonian, Upper Cretaceous, Mesozoic				
Ghul, Oman	no data		• coarse grained tabular cross-beds poorly-sorted rudstone hippuritids and gastropods	
		• structureless massive well-sorted medium sand-sized grainstone micritic clasts, radial oolites benthic foraminifers echinoderms coproliths, rare calcareous algae	• structureless massive well-sorted medium sand-sized grainstone micritic clasts, radial oolites benthic foraminifers echinoderms coproliths, rare calcareous algae	• structureless massive well-sorted medium sand-sized grainstone micritic clasts, radial oolites benthic foraminifers echinoderms coproliths, rare calcareous algae
Barremian, Lower Cretaceous, Mesozoic				
Cirque d'Archiane, Vercors, France *Middle wedge*	• 10 cm thick parallel beds bioclastic packstone/grainstone benthic foraminifers, gastropods green algae, echinoderm fragments	• wavy beds bioclastic packstone/grainstone benthic foraminifers, gastropods green algae, echinoderm fragments	• wavy beds bioclastic packstone/ grainstone benthic foraminifers, gastropods green algae, echinoderm fragments	• planar-laminated to wave rippled beds fine-grained packstone/wackestone foraminifers (miliolids, textularids), sponge spicules, quartz grains
La Montagnette, Vercors, France *Middle wedge*		• low-angle cross-beds poorly-sorted packstone miliolids, orbitolinids, lithoclasts fragments of green algae echinoderms	• HCS, swales, wavy beds medium sorted packstone orbitolinids, miliolids, bryozoans lithoclasts, fragments of green algae bivalves, gastropods, echinoderms	• well sorted wackestone miliolids, orbitolinids planktonic foraminifers fragments of echinoderms
Bajocian, Middle Jurassic, Mesozoic				
Vauchignon, Burgundy, France	no data	• low-relief coral bioherms	• low-angle cross-beds, undulatory beds crinoidal dominated grainstone/ rudstone bryozans, brachiopod spines, gastropods, bivalves encrusted by foraminifers, micritic coasting • bafflestone composed of dissolved corals	• undulatory bed surfaces, low-angle trough cross bedscrinoidal packstone • shaly layers with brachiopods
Vergisson, Burgundy, France	no data		• tabular cross-beds coarse-sand to gravel size grainstone	• well-sorted limestone median coarse size sand
Guadalupian, Permian, Palaeozoic				
Last Chance Canyon Area, NM, USA *LCC entrance, USA 5*[(1)]	no data	• cross-bedded ooid/peloid grainstone	• cross-bedded ooid/peloid grainstone	• massive dolomite-peloid wackestone/packstone
Panorama Point, USA 4[(2)]	no data	finely bedded : • fusulinid grainstone/packstone vertical burrows, Thalassinoides galleries • brachiopod-fusulinid wackestone	• brachiopod-fusulinid wackestone • fusulinid grainstone/packstone	• very silty brachiopod, sponde boundstone/wackestone
Baker Pen Draw, USA 3[(3)]		• fusulinid grainstone/packstone	• brachiopod-fusulinid wackestone	• microskeletal spical wackestone
Vendian, Proterozoic				
Zebra River Area Namibia	• trough cross beds poorly sorted grainstone and rudstone rich in intraclasts and composite ooids	graded composite beds composed of: • ooid grainstone with normal grading • fine-grained peloidal packstone capping ooid grainstone	• amalgamated HCS ($\lambda = 0.5$ m) grainstone omission surfaces	• shale layers • thin-bedded fine-grained limestone with some minor gutter casts • massive limestone beds capped by wave-related ridges and furrows

(1) Documentation from Weber, Kerans & Nance (1991) and own observations; (2) documentation from Sonnenfeld (1991) and own observations; (3) documentation from Sonnenfeld (1991), Sonnenfeld & Cross (1993).

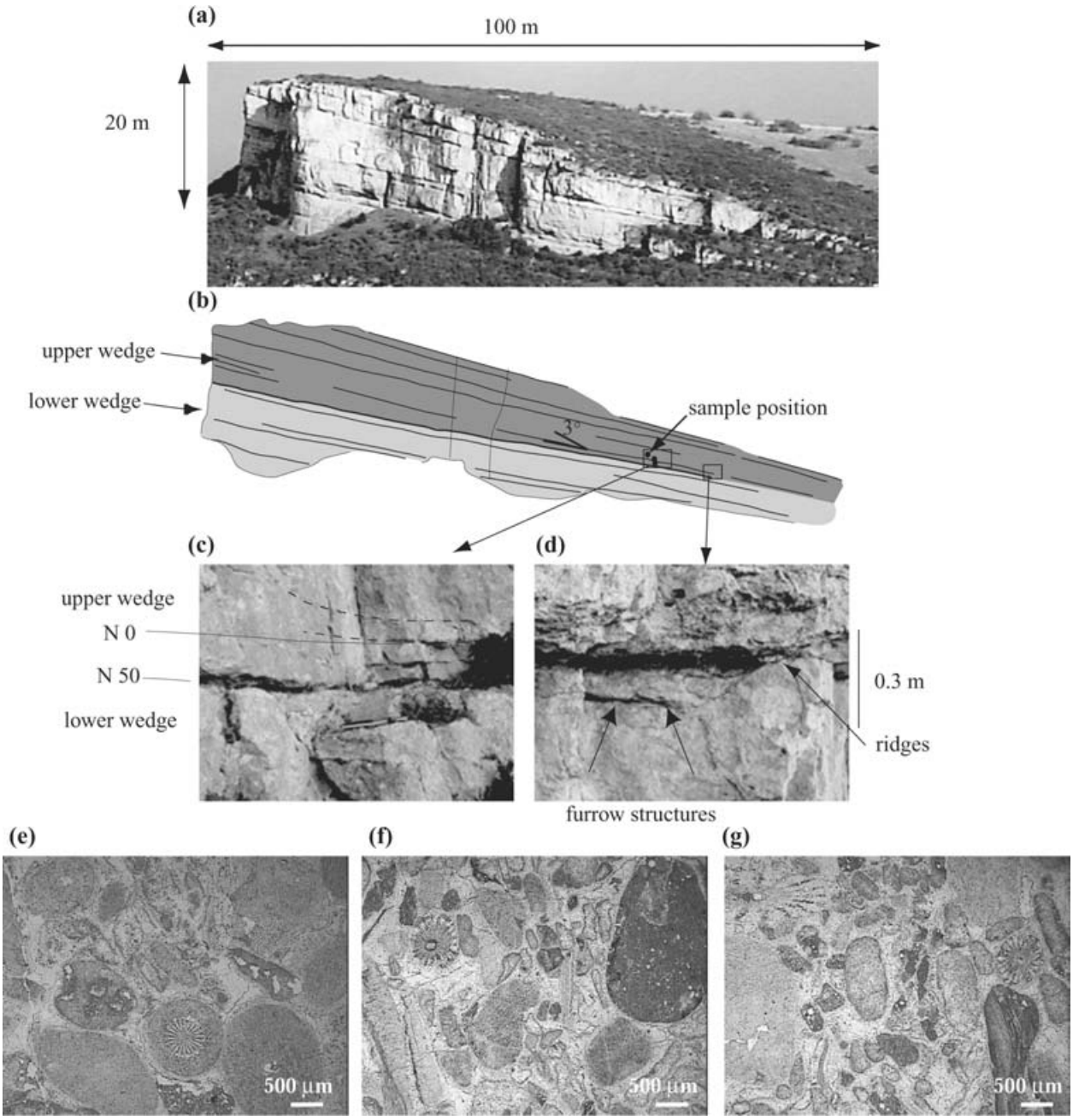

Figure 3. (a) Photograph and (b) line drawing of a pair of low-angle, oblique clinoforms at the Roche de Vergisson, South Burgundy, France (Lower Bajocian, Middle Jurassic). Outcrop close-up of depositional facies: (c) angular toesets at the bottom of the upper clinoform; (d) storm-generated furrow associated with the hiatal, downlap surface of the upper clinoform. Photomicrograph of grain-supported fabrics in the basal upper unit (dark grey): (e, f, g) gravel- to sand-sized crinoid ossicles, (e, f) coral pieces, (f, g) mollusc shell debris and (f) lithoclasts. Hammer length is 30 cm.

Clinobeds are 0.1–0.4 m thick wavy beds grouped into 2–10 m thick clinothems (Fig. 4c). Clinobeds are composed of bioclastic limestone and are intercalated with thin marl layers on the toe-of-slope (Fig. 4a). They are amalgamated and separated by hiatal or erosional surfaces on the middle and upper clinoform slope. The carbonate skeletal components consist of an open-marine biota dominated by benthic foraminifers and green algae (Fig. 4d–f; Table 1). Sediment fabrics range from wackestone to rudstone (Fig. 4d) and are dominantly packstone (Fig. 4e, f). Beds are commonly bioturbated.

Continuous lateral observations of facies across a single asymmetrical sigmoidal clinoform (Fig. 4b) show a well-zoned profile with evidence of upper-flow regimes (low-angle cross-beds) in the upper slope, and profuse structures of oscillatory flows (hummocky cross-stratification, swales, wavy beds) (Fig. 4c–f;

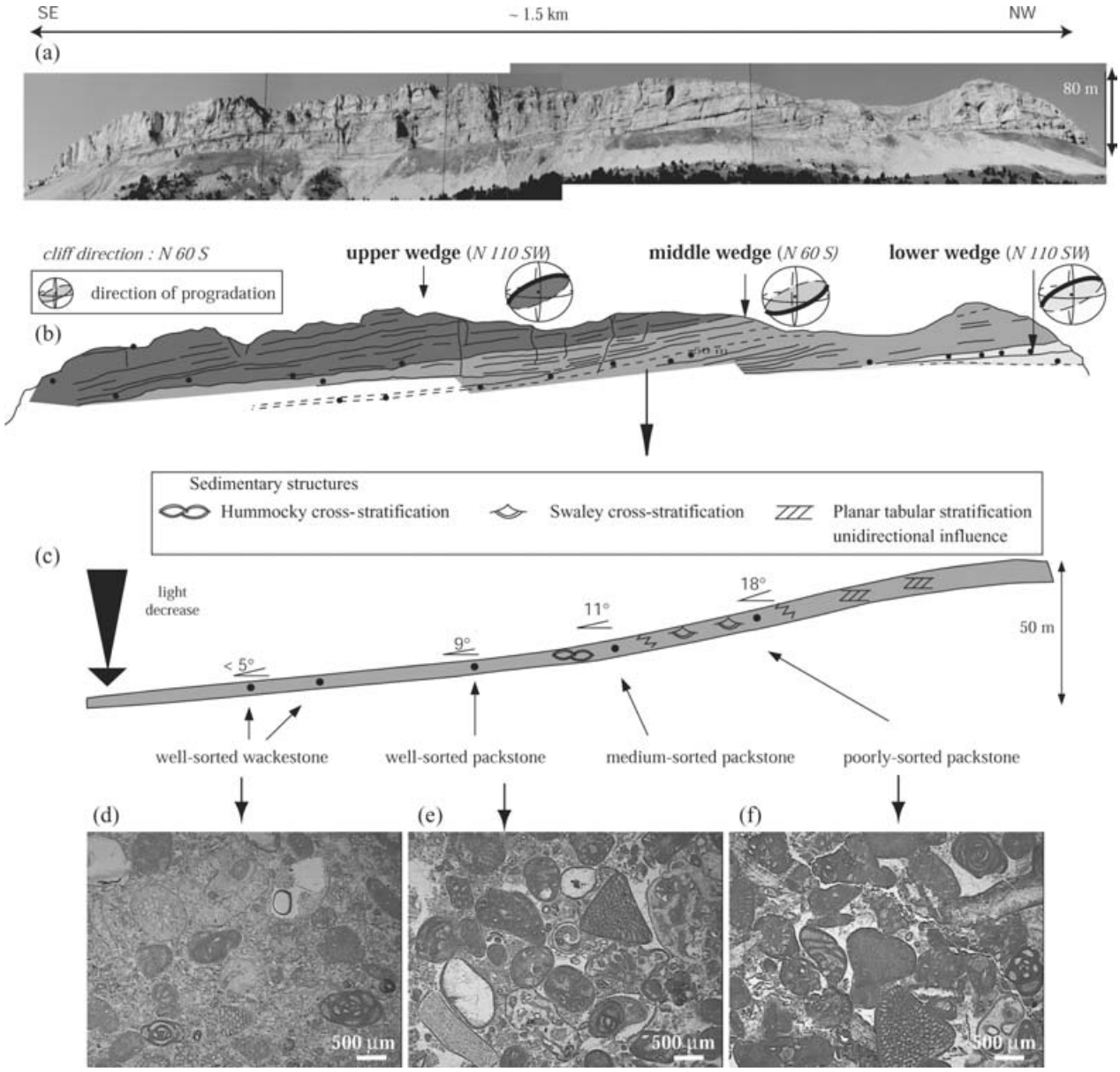

Figure 4. (a) Photograph and (b) line drawing of high-angle, asymmetrical sigmoidal clinoforms at La Montagnette, Vercors Plateau, France (Barremian, Lower Cretaceous). (c) Detailed profile and faciological attributes of a prominent clinoform in the middle wedge. (d–f) Photomicrographs of sediment fabrics along the clinoform. Note the pervasive matrix recrystallization (microspar), and the general increase in grain size towards the upper slope. (d) Toe-of-slope wackestone with benthic foraminifers (orbitolinids, robust miliolids), debris of calcareous algae, echinoderms, and bryozoans. (e) Lower slope packstone with orbitilinids, gastropod and echinoderm debris, and coated grains. (f) Middle slope packstone with orbitolinids, miliolids, gastropods, calcareous algae and lithoclasts.

Table 1) in the middle- and toe-of-slope. Grain-size decrease and rarefaction of green algae downslope are interpreted as reflecting decreasing hydrodynamic power and light penetration with increasing palaeo-water depth. The fair-weather wave-base position can be placed in the middle- to toe-of-slope transition, just beneath the last downward occurrence of swaley cross-beds (Fig. 4c). Identical facies assemblages through clinobeds have been observed vertically.

Based on sedimentary structures, biota and the regional facies tract, the Montagnette cliff is interpreted as reflecting a proximal shelf setting.

3.b. Distal clinoforms

3.b.1. Middle Jurassic Burgundy platform (Vauchignon) (Fig. 5)

The Vauchignon cliff, located south of Dijon, exposes distal clinoforms equivalent to the Roche de Vergisson.

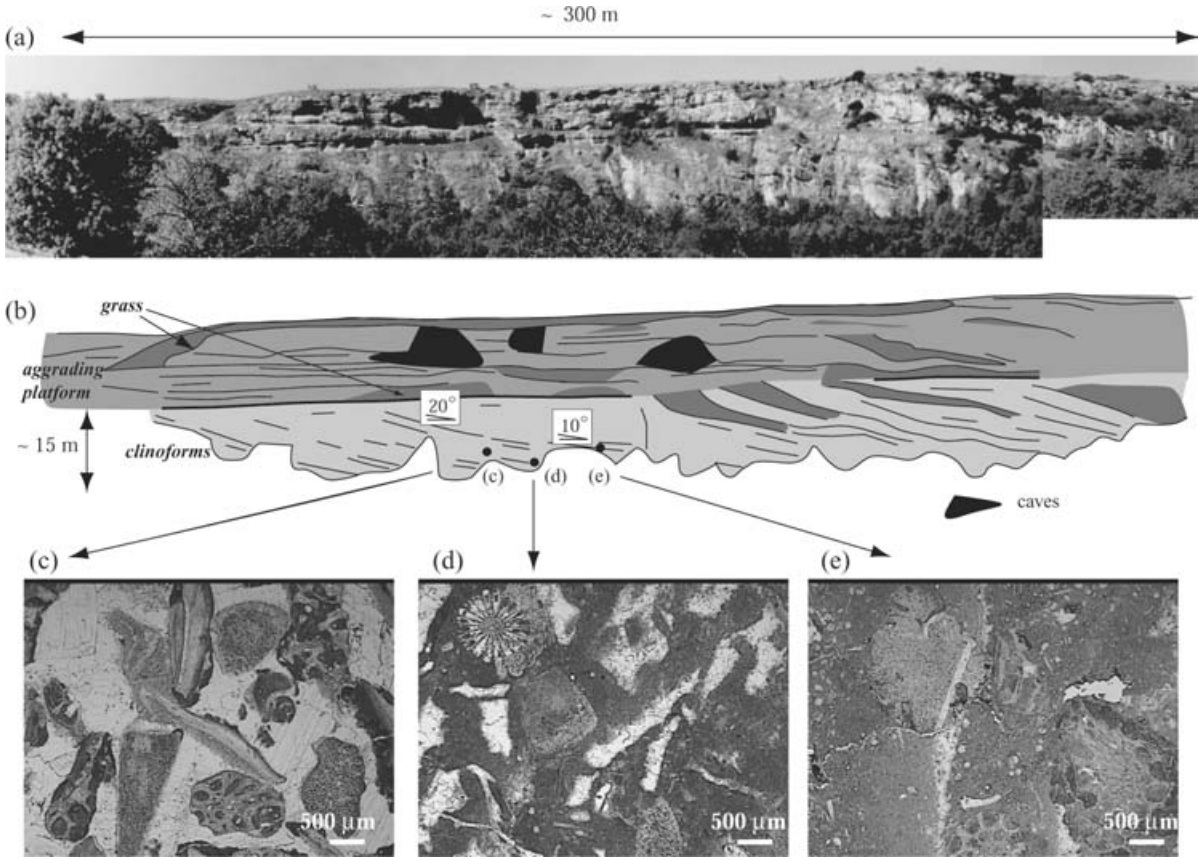

Figure 5. (a) Photograph and (b) line drawing of sharp-edged, exponential clinoforms at Vauchignon, Burgundy, France (Lower Bajocian, Middle Jurassic). The exposed section is slightly oblique in the direction of progradation, lowering the real dip of clinoforms. Photomicrographs of slope sediment fabrics: (c) middle-of-slope skeletal grainstone (bryozoan debris, crinoid ossicles, mollusc shells encrusted by nubecularids) and (d) coral bafflestone; (e) toe-of-slope packstone composed of coarse-sized bryozoan and crinoid debris floating in a matrix rich in sponge-spicules.

Clinoforms are traceable for over 300 m and have a height of about 15 m (Fig. 5). Clinoforms display a sharp-edged exponential profile with flat-topped truncation. Clinothems are composed of 4–5 m thick beds that pinch out basinwards to a few decimetres. The upper slopes are flanked by low-relief coral bioherms, and profiles are inclined up to about 25°. Two distinct facies were found in the middle to lower slopes (10° inclined beds): clinoform assemblages change vertically from crinoidal-dominated to bafflestone facies. Laterally, toesets are made up of crinoidal packstone separated by shaley layers yielding brachiopods. Facies assemblages along the Vauchignon are interpreted as representing distal clinoforms on a shelf-break setting.

3.b.2. Cirque d'Archiane (Fig. 6)

A second, stratigraphically younger, distally steepened ramp of the Vercors platform was also investigated at the base of the cliff on the western side of the Cirque d'Archiane belonging to the Barremian Glandasse Bioclastic Limestone Formation (Arnaud, 1981). Three depositional wedges were distinguished on the basis of the large-scale stratal pattern (Fig. 6a, b). Clinoforms in the lower wedge have a symmetrical sigmoidal shape and can be traced laterally over 50–80 m (Fig. 6b). Conversely, clinoforms from the middle and upper wedges display an asymmetrical sigmoidal pattern. The convex-upwards traces in the upper clinoform slope are laterally limited to a few tens of metres, whereas the concave-upward shape develops laterally over several hundred metres. The lower wedge and lower middle wedge exhibit toplap stratal termination, whereas clinoforms from the upper middle wedge show aggradation in the upper slope (conspicuous further north in Fig. 6a). Declivity at the inflection point is similar for the lower and middle wedges and is about 15°. Clinoforms exhibit about 40 m of relief from the top units to toe-of-slope. The upper wedge differs in its lower dip angles (~ 12°), considerable lateral extension (~ 1 km; see Jacquin *et al.* 1991 and Everts *et al.* 1995) and considerable relief (up to 100 m).

The cliffs at Cirque d'Archiane only allow field access to the middle- to toe-of-slope facies, which

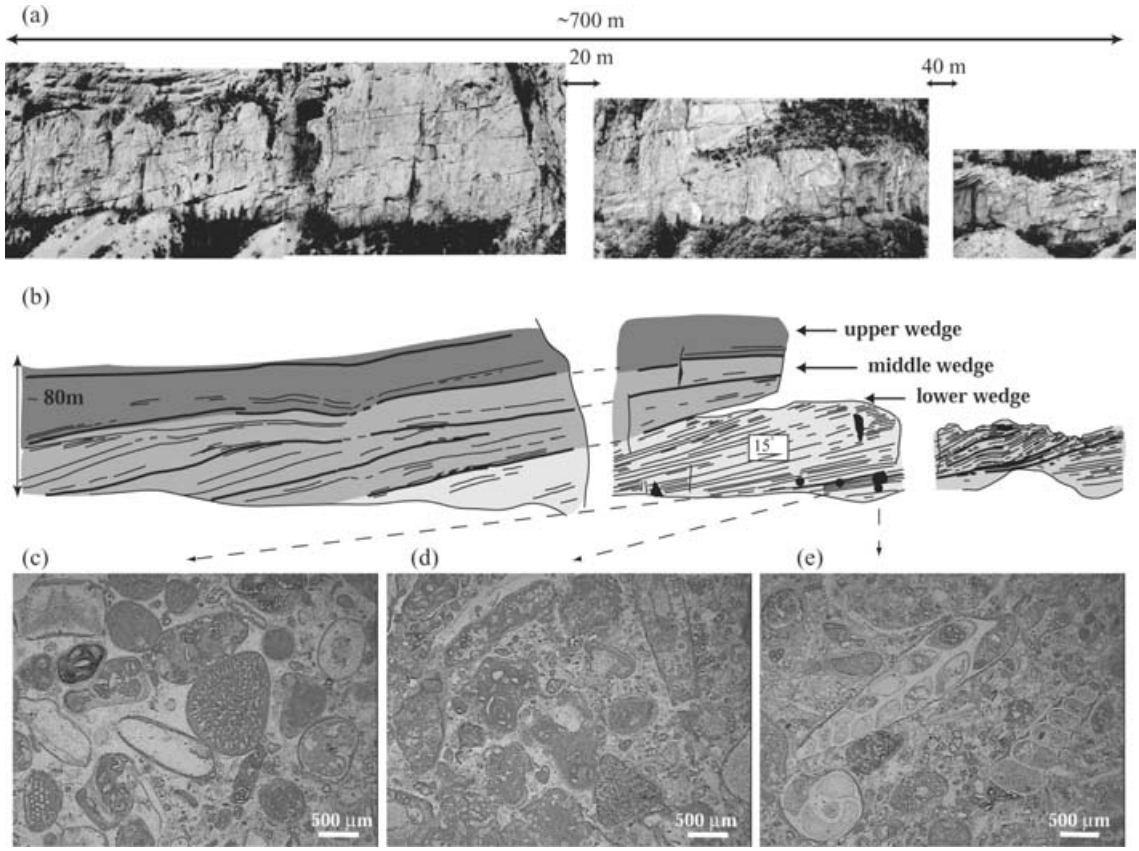

Figure 6. (a) Photograph and (b) line drawing of high-angle, symmetrical to asymmetrical sigmoidal clinoforms at Cirque d'Archiane, Vercors Plateau, France (Barremian, Lower Cretaceous). Photomicrographs of grain-supported, poorly sorted fabrics in the lower slope of clinoforms: grains are composed of (c) a mixture of limeclasts and (d) other lithoclasts, plus skeletal grains including typical platform-derived biota such as (c, d) conical orbitolinids, (c) robust miliolids, (e) gastropods and (c, d) calcareous algae.

exhibit similar sedimentary structures and biota in the three wedges (Fig. 6c–e; Table 1). Clinobeds are arranged in clinothems of dominantly bioclastic, grain-supported deposits. Skeletal grains are mostly composed of platform-derived benthic foraminifers, gastropods and green algae. Constituents also include grains present in any platform or basin environment, such as echinoderm fragments and diverse lithoclasts. Observations along clinoforms show that lateral facies differentiation evolves gradually without any abrupt change (Table 1). Flat-topped unit deposition is governed by laminar flow (10 cm thick parallel beds with a limited lateral extension of a few metres). Laterally, the middle clinoform slope deposits are formed by storm-induced oscillatory flows (e.g. wavy beds). The carbonate clinobeds at the toe-of-slope interfinger with marls basinwards. Clinoform toe facies, regionally referred to as 'calcaires hémipélagiques', are thin, planar-laminated to wave-rippled beds, interpreted as representing toe-of-slope clinoform sediment gravity flows below the storm wave-base, with initiation of flows on the clinoform slope (K. McDonough, unpub. Ph.D. thesis, Colorado Sch. Mines, 1997). No vertical facies evolution has been detected through beds.

3.b.3. Upper Cretaceous of northern Oman (Fig. 7)

This study site is located at the toe of the southwestern flank of Jebel Akhdar, close to the village of Ghul (23°09′ N, 57°12′ E), at the mouth of a valley referred to as Wadi Nakhr. The Lower Turonian section corresponds to the uppermost part of the Natih A Formation (Philip, Borgamano & Al-Maskiry, 1995) and represents the final carbonate system before nappe emplacement created the North Oman foredeep. The Lower Turonian rudist-bearing carbonate shelf developed over the Jebel Akhdar, dipping southwards to the Adam Foothills area, wherein basinal facies consist of chalky and cherty limestones (Van Buchem *et al.* 2002). The middle shelf facies, exposed further east in the El Hamra section, consist of fine-grained carbonate, rich in sponges and organized in decimetre-thick, graded storm-layers exhibiting long-wavelength undular lamination.

The middle- to outer-shelf transition is marked by short and oblique clinoforms downlapping onto a major hiatal surface that can be observed in the uppermost part of the Ghul cliff (Fig. 7a–c). The rocks below the hiatal surface are carbonate mudstone to sparse

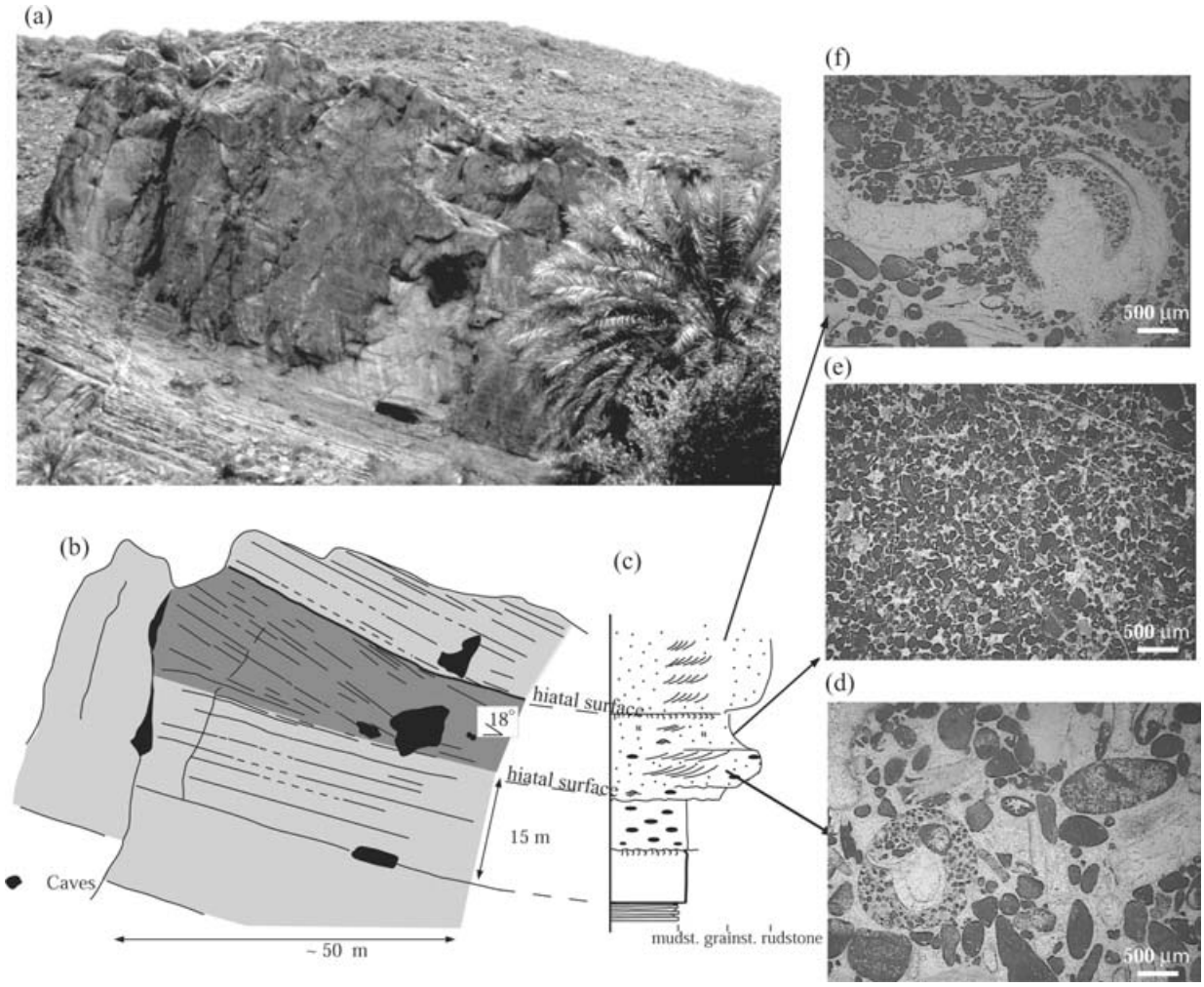

Figure 7. (a) Photograph and (b) line drawing of high-angle, oblique clinoforms in Wadi Nakhr, Jebel Akhdar, Oman (Turonian, Upper Cretaceous). (c) Textural log and (d–f) photomicrographs of grain-supported sediment fabrics showing highly contrasted vertical grain-size distribution. (d, f) Coarse grains include gastropod debris (moldic sediments and macrospar-replaced shells), limeclasts, robust miliolids, and echinoderm debris (syntaxial calcite overgrowth). (e) Fine sand-sized grains include peloids, fibro-radious oolites, and mini-foraminifera (miliolids).

wackestone. The overlying rocks, shown in dark grey in Fig. 7, form a prograding wedge of clinobeds with a maximum dip on the clinoform of 18°. Clinobeds are interpreted as lower-to-middle clinoform slope deposits. Clinoforms are composed of the vertical succession of two distinct facies (Fig. 7d–f; Table 1). The first facies consists of coarse-grained poorly sorted tabular cross-beds, showing transport by current traction combined with micro-avalanching. The corresponding sediment fabric is a poorly sorted rudstone comprising large fragments of hippuritids and gastropods (Fig. 7d, f). The second facies consists of structureless, well-sorted, medium sand-sized grainstone (Fig. 7e). This entire sequence is capped by a burrowed omission surface (Fig. 7b, c). This results in highly contrasted vertical facies differentiation. It was not possible to study lateral facies differentiation at this site.

3.b.4. Miocene of South Turkey (Figs 8, 9, 10)

The site studied is located north of Ermenek city (36°48′ N, 32°58′ E) in the Taurides Mountains of south-central Turkey, on the northwestern margin of the Cenozoic Mut Basin (Williams *et al.* 1995). Miocene carbonate deposits directly onlap folded Mesozoic rocks (Bizon *et al.* 1974) that were uplifted and heavily dissected during Oligocene times. Depressions were initially filled by Upper Burdigalian sediments. Subsequent Langhian carbonate systems colonized basement highs and started prograding in radial directions off the highs. The Ermenek site shows spectacular progradation of Langhian carbonate deposits into a several-kilometres-wide inshore basin lying behind a shallow water rim (X. Janson, unpub. Mémoire de DEA, Ecole Nationale Supérieure des Pétroles et Moteurs, 1997). Outcrop conditions permit

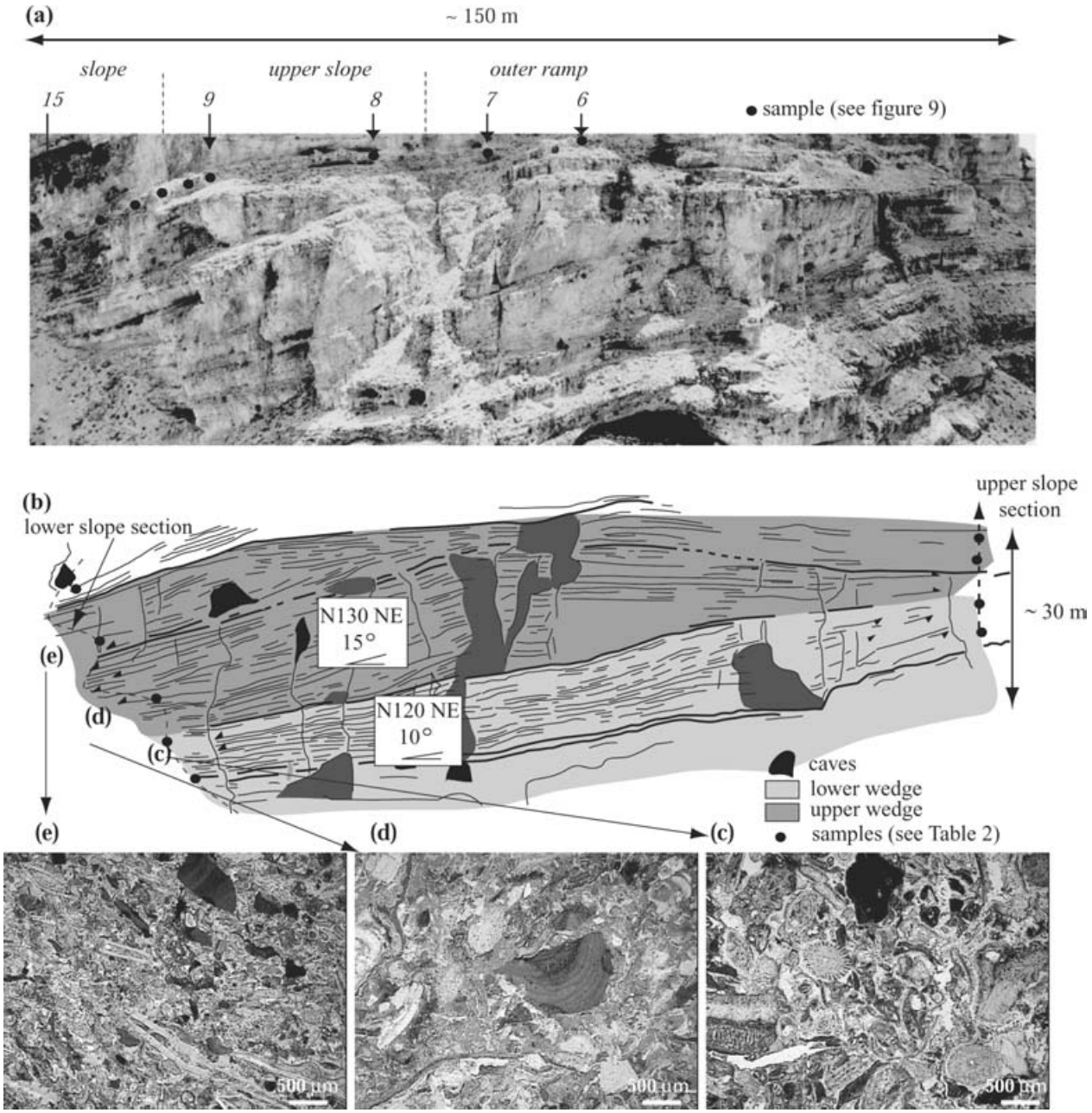

Figure 8. (a) Photograph and (b) line drawing of high-angle, oblique to sigmoidal clinoforms in the lower wedge, Ermenek platform, Turkey (Langhian, Miocene). (c–e) Photomicrographs of grain-supported fabrics in the lower slope of clinoforms (c) showing a general grain-size decrease along with progressive admixture of autochthonous biota (*Heterostegina*) (e) to ramp-sourced debris: *Amphistegina* (c, e), red algae (c, d, e), coral (c). Echinid and mollusc debris (c, d) are ubiquitous. The 19 samples in Table 2 were taken along a clinobed that veneers the upper unit, from toe-of-slope up to the outer ramp, over a horizontal distance of about 100 m.

a total sedimentary section about 250 m thick to be observed. Two examples of these progradation wedges are presented in detail.

The lower wedge (Fig. 8) is composed of two stacked units that both display oblique to sigmoidal-shaped clinoforms (Fig. 8a, b). The lower unit shows long, oblique to slightly concave-upwards clinoforms, whereas those of the upper unit are shorter and steeper (15° rather than 10°). Individual clinoforms exhibit between 20 to 25 m of relief for the lower and upper unit, respectively (Fig. 8).

Field conditions allow observation of facies in toe-of-slope and upper clinoform slope sections. Facies descriptions of lower and upper slope sections are shown in detail in Table 2. Top and onlapping strata on both units of the upper clinoform slope are stacked and compose a massive, medium- to coarse-grained unit rich in rhodolites, corals, bryozoans, echinoid fragments and benthic foraminifers (see Table 2, upper slope section). Sediment fabrics are uniformly grainstone on the lower unit and change vertically from grainstone to wackestone to boundstone on the

Table 2. Sedimentary structures, sediment fabrics and constituents of lower slope (left) and upper slope (right) sections in ascending stratigraphic order through progradation and retrogradation units in the lower wedge, Miocene, South Turkey (see Fig. 8b)

Lower slope section (1)					Upper slope section (3)
Sedimentary structures	Sediment fabrics (2)	Sorting	Grain-size (mm)	Bioclastic components	Bioclastic components
Upper unit					
symmetrical ripples megaripples wavy bedding horizontal burrows	mudstone	very good	0.5–1	benthic foraminifers (small-sized Heterostegina)	echinoids debris (A) coral mollusc shell debris (C) red algal debris (C)
planar lamination	packstone	medium	0.5–1	*red algal debris (A) mollusc shell fragments (C) echinoid debris (C) benthic foraminifers (R) (alveolinids-*gypsinids-*Amphistegina) benthic foraminifers (A) Heterostegina planktic foraminifers (C) globigerinids	echinoids debris (C) benthic foraminifers (R) benthic foraminifers (A) Heterostegina=Amphistegina>discorbids bryozoans (C) echinoids debris (C) planktic foraminifers (R) globigerinids
wavy bedding	packstone (e)	good	0.5–1	bryozoans (C) echinoid debris (C) *minute red algal debris (R)	
furrows and ridges	packstone	poor to good	0.5–5	*red algal debris (C) *coral debris (C) mollusc shell debris (C) benthic foraminifers (R) (*gypsinids-textularids-*Amphistegina) planktic foraminifers (R)	red algal debris (A) benthic foraminifers (A) Heterostegina=Amphistegina=gypsinids>alveolinids echinoids debris (C) red algal debris (A) benthic foraminifers (A) Amphistegina=gypsinids red algal debris (A) benthic foraminifers (A) Amphistegina=gypsinids>Heterostegina echinoids debris (A)
oyster-rich levels graded beds gutters	packstone to grainstone (d) to rudstone	poor to very poor	0.5–10	*red algal debris (C) echinoid debris (C) mollusc shell debris (C) benthic foraminifers (C) (Heterostegina=*Amphistegina) bryozoans	benthic foraminifers (C) Heterostegina>gypsinids coral mollusc shell debris (C)
Lower unit					
planar lamination furrows	grainstone (c)	medium	0.5–2	*red algal debris (C) echinoid debris (C) mollusc shell debris (C) benthic foraminifers (C) (*Amphistegina>Heterostegina=*gypsinids)	red algal debris (A) benthic foraminifers (A) gypsinids>Heterostegina echinoids debris (A) red algal debris (A) benthic foraminifers (A) operculinids
amalgamated beds sand mounds	rudstone	very poor	0.1–10	*red algal debris and rhodolites (C) *coral debris (C) large mollusc shells (C) (pectinids, Oysters, *Gastropods *echinoid spines (C) benthic foraminifers (C) (alveolinids>miliolids>*Amphistegina	echinoids debris (A) red algal debris (A) benthic foraminifers (A) operculinids>Amphistegina echinoids debris (A)

*upper slope- and outer ramp-derived bioclastic components; (A) – abundant; (C) – common; (R) – rare.
(1) Section shown in Figure 8; (2) sample lettering c, d, e as used in Figure 8b; (3) Section located about 50 m to the right of area shown in Figure 8a.

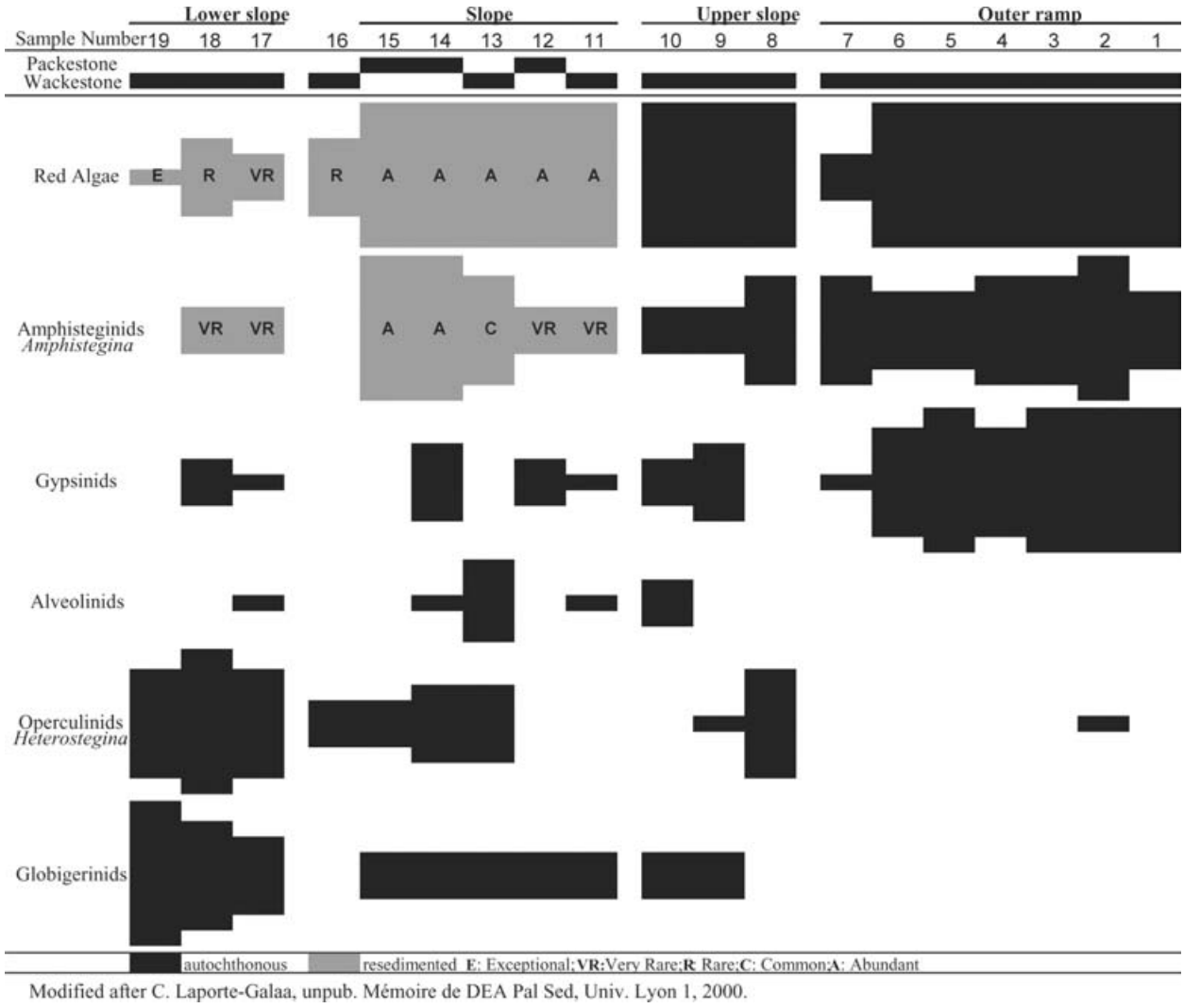

Figure 9. Distribution of the biotic assemblage (red algae and foraminifers) across a clinoform that veneers the upper unit of the lower wedge, Miocene, South Turkey (see Fig. 8). This distribution reflects the ecological distribution of carbonate biota along the ramp.

upper unit. The lower slope stratal assemblage of both units is made up of 3 to 5 m thick clinothems, which are themselves composed of 0.2 to 0.5 m thick individual clinobeds. The clinoforms are each bounded by major omission or erosion surfaces. Sediment fabrics within the lower slope range from packstone to rudstone and some mudstones that are rich in red-algal debris and benthic foraminifers (*Heterostegina*, Amphisteginids). Bryozoans and scaphopod clasts are ubiquitous (see Table 2, lower slope section). Planar laminated grainstones and amalgamated beds of rudstones dominate the lower unit, leading to a uniform vertical facies differentiation in the lower unit. The vertical sequence of lithologies and sedimentary structures varies significantly in the upper unit. Graded beds of grain-supported textures and packstones dominate the upper unit but abrupt changes from grainstones to packstones, and some mudstones, have been observed. This results in highly contrasted vertical facies differentiation in the upper wedge (Table 2). Comparison between upper and lower slope sections suggests poor lateral facies differentiation in the lower unit and gradual lateral facies differentiation in the upper unit (Table 2).

Successive observations along an individual clinoform yield data on lateral facies variation down the clinobeds in the upper unit (C. Laporte-Galaa, unpub. Mémoire de DEA Pal Sed, Univ. Lyon 1, 2000) (Fig. 8). One sigmoidal to oblique clinobed that veneers the upper unit was closely and regularly sampled from the toe-of-slope up to the outer ramp, over a horizontal distance of about 100 m (Fig. 8). Sediment fabrics and grain composition of samples from the upper unit are reported in Fig. 9. The distribution of biota and the very weak lateral thickness variation of the bed are both indicative of limited downslope resedimentation of carbonate grains. This clinoform is assumed to have recorded the original ecological distribution of

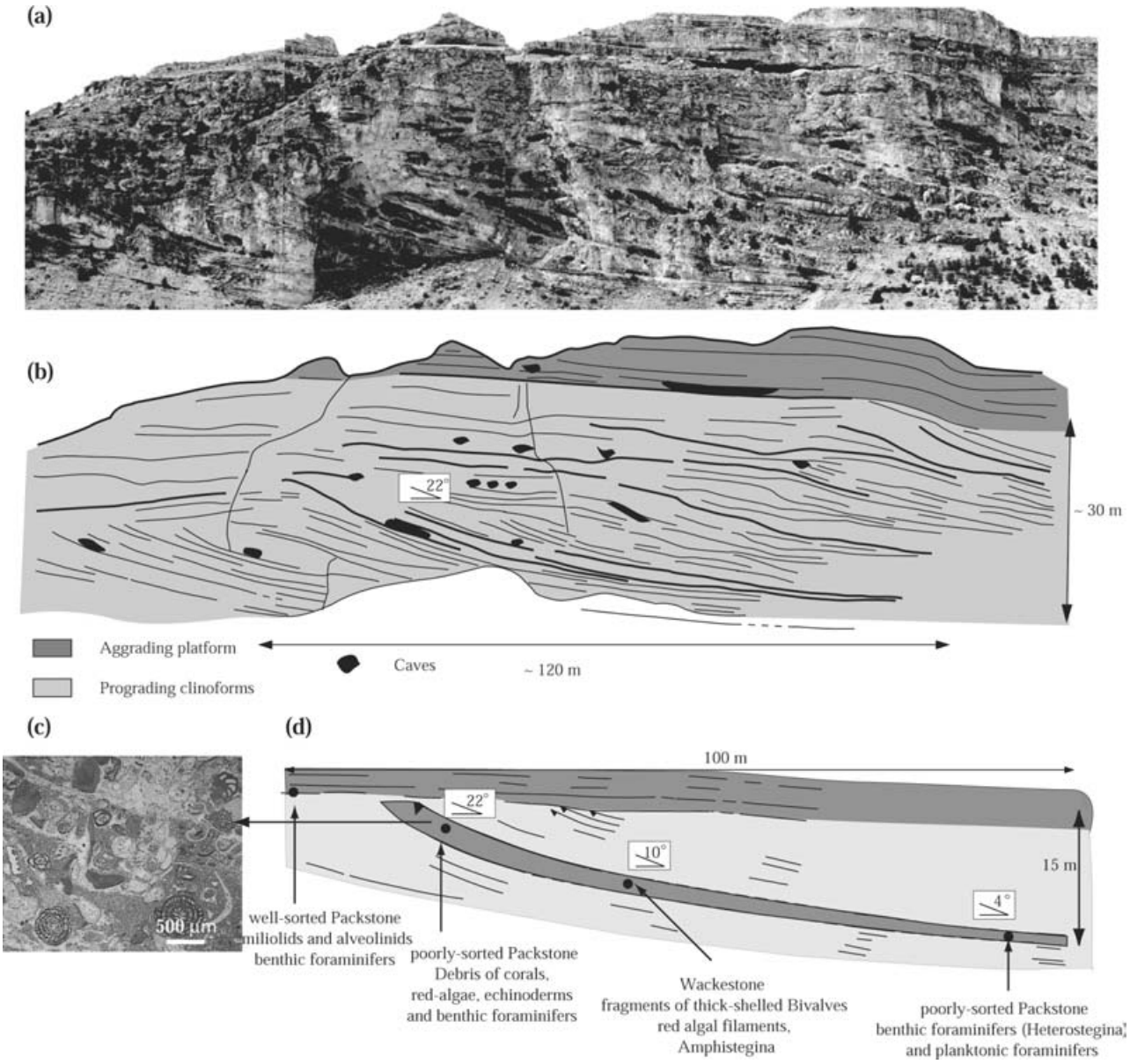

Figure 10. (a) Photograph and (b) line drawing of high-angle, exponential clinoforms of the upper wedge, Ermenek platform, Turkey (Langhian, Miocene). (c) Photomicrograph of a wackestone/packstone fabric in the upper lower slope of the upper wedge Ermenek platform, Turkey (Langhian, Miocene). Benthic foramifera are *in situ* alveolinids (*borelis melo*), and transported miliolids and *perenoplis* sp. The reworked component includes red algal debris and clasts encrusted by bryozoans. (d) Depositional facies types across the slope.

carbonate biota along the distal ramp. The mollusc and echinoderm debris are common and ubiquitous along the clinoform. Conversely, the outer ramp and upper slope of the clinoform is marked by abundant autochthonous red algae and large benthic foraminifers. Alveolinids and operculinids are restricted to the lower and middle portion of the clinoform, and occur with transported red algae and amphisteginids. This observation is consistent with the fact that, in modern settings, the *Heterostegina* genus is abundant between 40 and 70 m water depth (Hottinger, 1997).

The upper wedge (Fig. 10) displays an assemblage of concave-up, sharp-edged exponential clinoforms with top truncation terminations. Clinoform height can attain 30 m and declivity is up to 25° (Fig. 10a, b). Major omission surfaces delimit packages a few metres thick, composed of massive groups of amalgamated and parallel carbonate beds and thin shales. One of these clinoforms is entirely accessible on the opposite valley (Fig. 10c). From the flat-topped unit to toe-of-slope, the clinoform facies gradually evolves laterally from a well-sorted packstone containing abundant miliolids to a poorly sorted packstone bearing abundant amphisteginids, common operculinids and rare planktonic foraminifers. In the lower slope, facies evolve vertically from wackestone to grainstone

through clinothems, suggesting pronounced vertical facies differentiation.

4. Results

In the section below, we synthesize geometric observations (shape, declivity, height), and faciological analyses (sediment fabric, lateral facies differentiation and vertical facies differentiation) assessed on low-relief clinoforms. We also present cross-correlations between these parameters to extract the characteristics of low-relief clinoforms, and compare them to well-known high-relief clinoforms. Data from our case histories are supplemented below with data from Sonnenfeld (1991) and Weber, Kerans & Nance (1991) from the Permian carbonate ramp in the Last Chance Canyon area of New Mexico, USA. All data are summarized in Table 3.

4.a. Geometry: shapes, slope angles and height (Fig. 11)

Observed carbonate clinoforms display a large spectrum of profiles distributed between the three end-member shapes: oblique, sigmoidal and exponential. The most common form is the asymmetrical sigmoidal (Fig. 11). Maximal slope angles of studied clinoforms range from 3 to 25° (Fig. 11). Cross-correlation of shape and maximum angle reveals that sharp-edged exponential clinoforms exhibit the strongest declivities, about 25°. Sigmoidal shape is associated with 12–22° declivities, with the most common value around 15°. Asymmetrical sigmoidal clinoforms show low declivity, for example, 5° in the Neoproterozoic of Namibia, as well as high slope angles, and 18° in the Montagnette. Slope angles of oblique clinoforms display a great range of declivities, from 3 to 20°. Our dataset therefore suggests that there is no simple correlation between maximum slope angle and clinoform morphology, except for exponential clinoforms. Additional evidence of this independence comes from the Lower Cretaceous of the Cirque d'Archiane for which the clinoform profile clearly evolves while maximal slope angle does not change significantly (15°) (Fig. 6).

Clinoform height ranges from 5 to 100 m (Fig. 11). Oblique clinoforms display low-relief values ($< \sim 25$ m) with low variability, from 5 to 25 m, with relatively low slope angles. Exponential clinoforms are associated with 15 to 25 m of relief, and show the highest slope angles. Sigmoidal clinoforms display a great range of relief, from 20 to 100 m, most of them being grouped between 20 and 50 m, with intermediate slope values commonly around 15°. High relief (> 40 m) is only achieved with sigmoidal clinoforms, be they asymmetrical or symmetrical. Our dataset therefore suggests that oblique low-relief clinoforms exhibit lower relief than sigmoidal ones (Fig. 11), which differ from high-relief clinoforms (Keim & Schlager, 1999; Adams *et al.* 2002).

Sigmoidal patterns have elsewhere been proved to be a very common shape in low-relief clinoforms (e.g. uppermost Cretaceous in Italy: Eberli *et al.* 1993; Vecsei, 1998), but also in high-relief clinoforms (Carboniferous in Spain: Bahamonde, Colmenero & Vera, 1997; Lower Jurassic in Morocco: Kenter & Campbell, 1991), as well as in modern slope profiles (Adams & Schlager, 2000). Assessed slope angles are in good agreement with measurements made on clinoforms on a carbonate ramp in Menorca (12–20°) (Pomar, Obrador & Westphal, 2002). The large variability in our measured slope angles is also consistent with measurements published by Schlager & Camber (1986) for limestone escarpments.

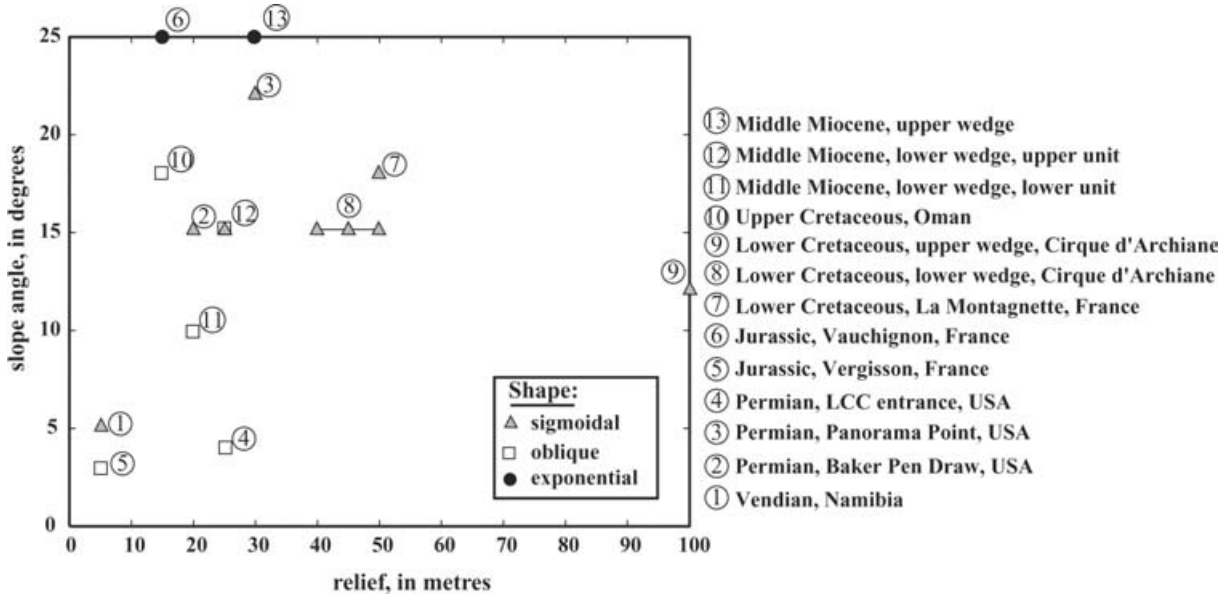

Figure 11. Plot of slope angle against relief for various shapes. LCC – Last Chance Canyon (USA).

Table 3. Synthetic features for the granular clinoforms of studied ancient carbonate shelves

Age/location	Shape	Height (m)	Maximum angle (°)	Sediment fabric	Lateral facies differenciation	Vertical facies differenciation	Dominant component	Depositional environment
Langhian, Miocene, Cenozoic								
Ermenek, Taurus, Turkey								
Upper wedge	Exponential	30	24	Pack	Gradual	Significant	B.F.	Distal shelf
Lower wedge, upper unit	Obl. to Sig.	25	15	Mud-Rud	Gradual to Pronounced	Significant	B.F.	Distal ramp
Lower wedge, lower unit	Obl. to Sig.	20	10	Gr-Rud	None	None	Red algae	Distal ramp
Turonian, Upper Cretaceous Mesozoic								
Ghul, Oman	Oblique	>15	18	Gr-Rud	Unobserved	Significant	B.F. (miliolids)	Distal shelf
Barremian, Lower Cretaceous, Mesozoic								
Cirque d'Archiane, Vercors, France	.							
Upper wedge	Asym. Sig.	>100	12	Gr	Gradual	None	B.F. (orbitolinids)	Distal ramp
Upper middle wedge	Asym. Sig.	40	15	Gr	Gradual	None	B.F. (orbitolinids)	Distal ramp
Lower middle wedge	Asym. Sig.	45	15	Gr	Gradual	None	B.F. (orbitolinids)	Distal ramp
Lower wedge	Sigmoidal	>50	15	Gr	Gradual	None	B.F. (orbitolinids)	Distal ramp
La Montagnette, Vercors, France								
Middle wedge	Asym. Sig.	50	18	Pack	Well-zoned	None	B.F. & green algae	Proximal shelf
Bajocian, Middle Jurassic, Mesozoic								
Vauchignon, Burgundy, France								
Lower wedge	Exponential	18	25	Gr-Rud	Gradual	Significant	Crinoids	Distal shelf
Vergisson, Burgundy, France	Oblique	>5	3	Gr	Gradual	None	Crinoids	Proximal shelf
Guadalupian, Permian, Palaeozoic								
Last Chance Canyon Area, NM, USA								
LCC entrance, USA 5[(1)]	Oblique	25	4	Gr	Unobserved	Weak	Ooids	Proximal ramp[(4)]
Panorama Point, USA 4[(2)]	Asym. Sig.	30	22	Wack-Gr	Unobserved	Significant	B.F. (fusulinids)	Distal ramp[(4)]
Baker Pen Draw, USA 3[(3)]	Asym. Sig.	20	15	Pack-Gr	Gradual	Weak	B.F. (fusulinids)	Distal ramp[(4)]
Vendian, Proterozoic								
Zebra River Area, Namibia	Asym. Sig.	5	5	Gr	Well-zoned	Unobserved	Ooids	Proximal ramp

Asym. Sig. – Asymmetrical sigmoidal; B.F. – benthic foraminifers; Gr – grainstone; Obl. to Sig. – Oblique to sigmoidal; Pack – packstone; Gr-Rud – grainstone to rudstone; Wack-Gr – wacke- to grainstone; Pack-Gr – pack- to grainstone; Mud-Rud – mud- to rudstone.
(1) Documentation from Weber *et al*. (1991) and own observations; (2) documentation from Sonnenfeld (1991) and own observations; (3) documentation from Sonnenfeld (1991) and Sonnenfeld & Cross (1993); (4) documentation from Kerans, Jerry Lucia & Senger (1994).

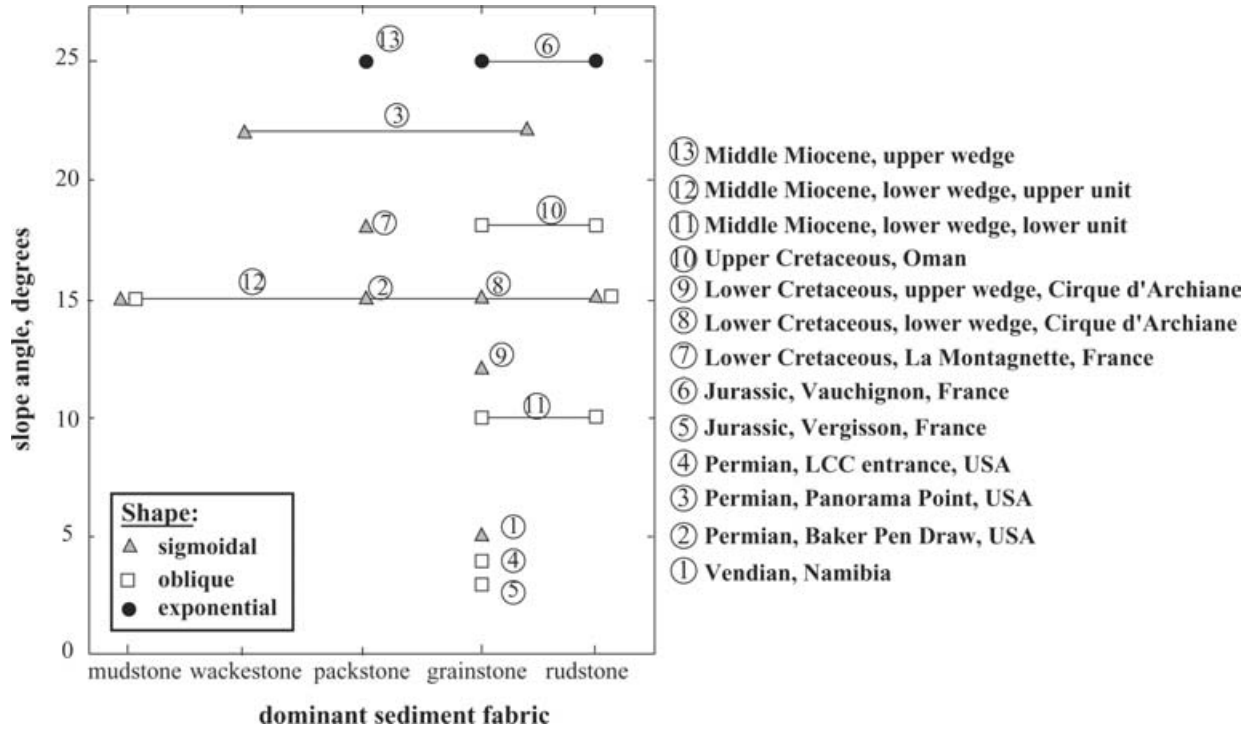

Figure 12. Plot of slope angle against sediment fabric for various shapes. LCC – Last Chance Canyon (USA).

4.b. Sediment fabric (Fig. 12)

Whatever the clinoform shape, most sediment fabrics are granular and grain-supported, that is, packstone, grainstone and rudstone. The occurrence of mud-dominated sediment fabric, that is, mudstone and wackestone, is rare in a clinoform upper slope, with the exception of the upper unit of the lower wedge, Miocene, Turkey (Fig. 9). The occurrence of the most granular, grain-supported fabrics, and of the coarsest-grained sediment, often coincides with the position of maximum declivity along the clinoform. This has been observed in the Montagnette and lower wedge (Turkey) cases and documented for linear flanks of high-relief carbonate platforms by Kenter (1990), Bahamonde, Colmenero & Vera (1997) and Keim & Schlager (1999). However, a cross-plot of sediment fabric versus maximal slope angle for carbonate clinoforms in shallow marine settings reveals clear scattering and no clear linear correlation between these parameters (Fig. 12; Table 3). Indeed, distinct sediment fabrics can be encountered through stacked clinobeds with an identical declivity, as in the Upper Cretaceous (Oman), and the lower wedge, upper unit and upper wedge (Turkey).

Our compilation is thus inconsistent with what has been stated for the linear flanks of high-relief carbonate clinoforms by Kenter (1990) and Adams & Schlager (2001). The slope angles of low-relief clinoforms cannot simply be related to the depositional angle and thus to the angle of repose. This discrepancy between low- and high-relief clinoforms probably comes from the type of depositional setting, and more specifically from the main transport mechanisms. Here, low-relief clinoform accretion seems to be primarily influenced by wave-induced sediment transport, as is shown by the numerous wave-induced sedimentary structures (see next Section). Conversely, high-relief clinoforms have been proved to be systems that build to the angle of repose, and for which gravity is the primary transport process (Kenter, 1990; Adams *et al.* 2002).

4.c. Facies differentiation (Fig. 13)

Great variety in lateral facies differentiation along clinoforms has been observed, from (1) well-zoned profiles, characterized by high facies contrast along individual clinoforms, to (2) gradual transitions, to (3) almost uniform facies (Fig. 13). Gradual lateral facies changes, for which the structures, sediment fabrics and biota all gradually evolve along the clinobed, are the most common. Lateral facies uniformity is exemplified by the Archiane case study and the lower unit of the lower wedge in Turkey (Figs 6, 8; Table 1). In contrast, well-defined facies belts have been encountered in the Montagnette, Namibia and Turkey case studies. Such pronounced facies evolution may result from hydrodynamic zonation with increasing water depth as has been shown in the cases of Namibia and La Montagnette, where planar-laminated facies induced by upper regime flows have been observed in the upper

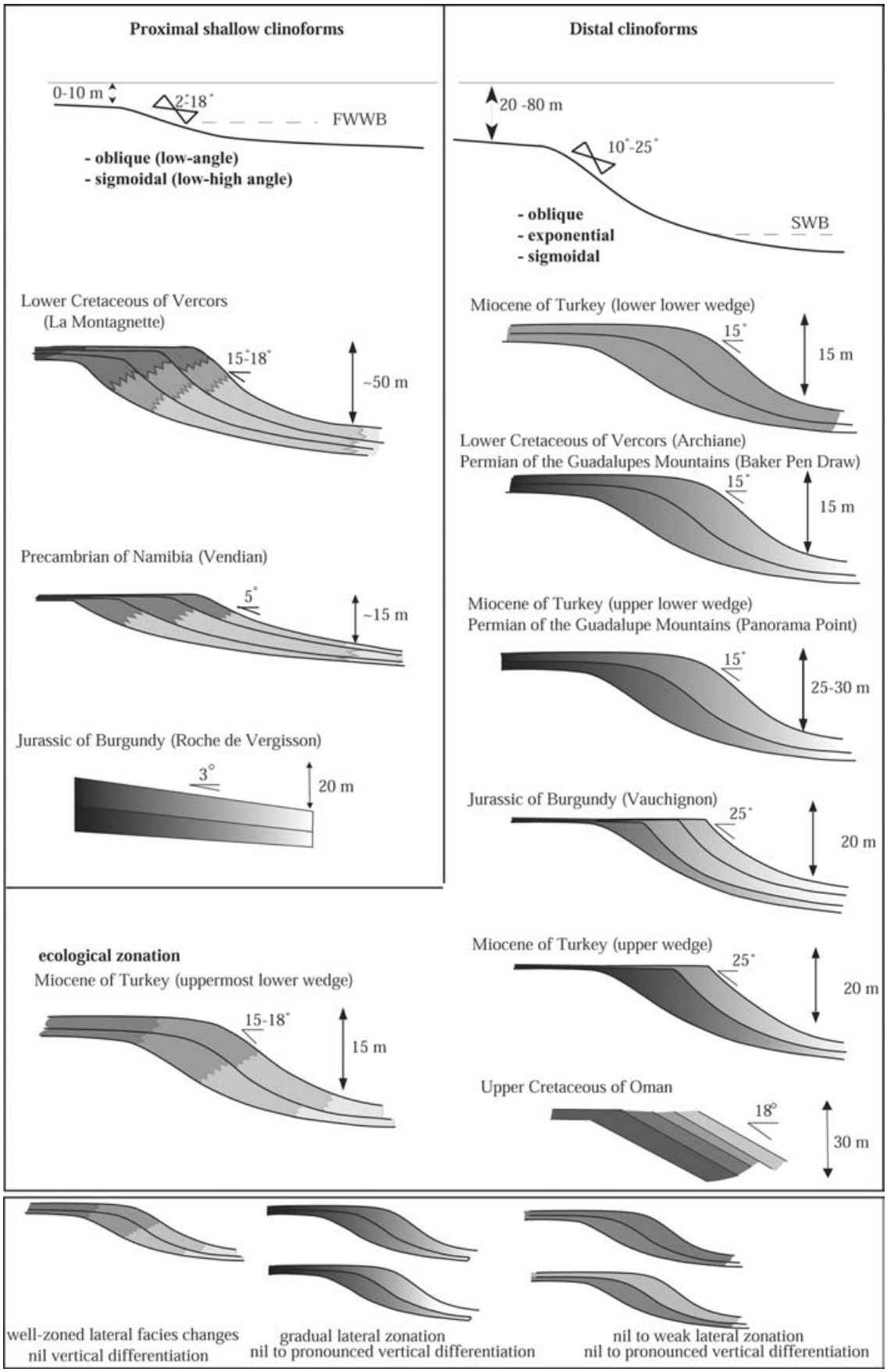

Figure 13. Schematic and synthetic diagram showing relationships between depositional environments, depositional profiles, lateral and vertical facies differentiation.

clinoform slope, and sedimentary structures induced by oscillatory currents have been encountered in the middle to lower slope. Pronounced facies evolution may also result from ecological distribution of carbonate biota along the slope, as has been described in the upper unit of the lower wedge in the Miocene (Turkey).

Clinoform vertical facies differentiation is often limited, with the exception of Vauchignon, Oman and the lower wedge (Turkey) cases for which highly contrasted vertical facies differentiation has been observed. Vertical facies differentiation may be explained by incremental vertical clinoform accretion induced by intermittent currents, as exemplified in Oman, where vertical evolution of poorly sorted rudstone facies showing cross-beds to structureless massive beds with no evidence of any strong currents, has been observed. Pronounced vertical facies differentiation may also result from the development of local coral buildup leading to a vertical succession of packstone to bafflestone facies, as is the case in Vauchignon.

Figure 13 shows that facies differentiation is not directly related to clinoform shape, height, or declivity, with the possible exception of oblique forms which are prone to display lateral uniformity, as in the Cretaceous (Oman) and in the Miocene, lower wedge, lower unit (Turkey).

As to the fundamental characteristics of low-relief clinoforms, it appears that storm-generated deposits (e.g. wavy beds, swales and hummocky cross-stratification) are very common features, whereas only rare local gravitational transport, induced by high-energy events, has been observed. This suggests that low-relief clinoform accretion occurs above the storm wave-base and is probably governed by wave-induced flows, more than by gravity transport, as has been established for high-relief clinoforms (Mullins *et al.* 1983; Kenter, 1990; Eberli, 1993; Adams & Schlager, 2000).

5. Discussion

In this section, we sort geometric and faciological characteristics of clinoforms relative to their depositional setting to discuss the influence of the environmental processes involved in clinoform accretion (Fig. 13).

5.a. Characteristics and accretion processes of proximal/shallow clinoforms

Proximal/shallow clinoforms show oblique (Roche de Vergisson, Burgundy, Fig. 3) to markedly asymmetrical sigmoidal forms (La Montagnette, Vercors, Fig. 4). Depositional angle values show two distinct categories: (1) low-relief features (< 5 m) with low-angle slopes ($< 5^\circ$) flanking coarse-grained flat shoals (Namibia, Fig. 2), and (2) medium-relief features (< 50 m) associated with higher slopes (15–18°) yielding the typical sedimentary structures of a permanently wave-agitated zone (La Montagnette, Vercors, Fig. 4). Whatever the slope, the sediment fabrics and sedimentary structures change in stages along this type of clinoform, leading to well-zoned lateral facies differentiation related to hydrodynamic zonation: evidence of unidirectional flows (e.g. cross-beds) is pervasive on the flat upper clinoforms, whereas marks of storm-generated oscillatory flows, such as hummocky cross-beds, dominate in the middle- and toe-of-slope. Maximum declivity of the middle–upper slope coincides with the occurrence of combined flows (La Montagnette, Vercors). Conversely, vertical facies differentiation through this type of clinoform, for a given position on the slope, is limited, suggesting that clinoforms are built up by the repetitive stacking of relatively similar, single clinobeds. Additionally, the general architecture of these clinoforms shows that they were formed by the amalgamation of deposits in high-energy conditions, as is evidenced by the pervasive presence of storm-related features like hummocky cross-stratification, planar laminations, etc.

There are two non-mutually exclusive possibilities to account for the difference between low- and high-relief proximal/shallow clinoforms: hydrodynamics and sediment production. The upper parts of low-relief forms contain coarse-grained (gravel-size) debris (e.g. composite ooids and crinoid ossicles), whereas high-relief counterparts contain a substantial amount of typical light-dependent biota (green algae in the Lower Cretaceous of La Montagnette). It is hypothesized that the low-relief forms reflect hydrodynamic equilibrium profiles, in the sense proposed by Swift & Thorne (1991). Such low-relief forms should thus reflect a balance between sediment production and transport efficiency by waves and currents. Conversely, high-relief forms could be primarily indicative of the rapid decrease in carbonate sediment production rate with water depth.

5.b. Characteristics and accretion processes of distal clinoforms

Distal clinoforms show a great variety of profiles, but their angles are apparently restricted to within the 10 to 25° range (Fig. 13). Most of the coarse-grained sediment in the clinoforms derives from carbonate biota of the middle shelf and upper slope: crinoids, red algae, benthic foraminifers. The contribution by *in situ* skeletal production becomes significant in the toe-of-slope only: brachiopods (Permian, Jurassic), sponges (Permian, Jurassic, Lower Cretaceous), bryozoans (Permian, Jurassic), deep-water benthic foraminifers (textularids for the Lower Cretaceous, operculinids for the Miocene).

Lateral facies differentiation along these clinoforms is either nil or gradual, but never yields well-achieved zonation along the slope. Vertical facies differentiation

through clinobeds is either nil (e.g. Lower Cretaceous, Archiane) or very contrasted (e.g. Upper Cretaceous, Oman). Clinoforms show occasional evidence of laminar (lower unit, Archiane) and unidirectional (Upper Cretaceous, Oman) flows. Conversely, marks of oscillatory flows (undular, wavy top bounding surfaces of clinobeds) are common in the lower slope settings of the Middle Jurassic (Vauchignon), Lower Cretaceous (Archiane) and Miocene (Turkey) (lower unit of the lower wedge). These variations in structure suggest that clinoforms build from sediment transport by waves and currents on top sets and upper slopes, and by oscillatory flows on the lower slopes.

The analyses of clinofacies reveal that clinoforms developed between the fair- and storm-weather wave-base and were built out by sediment swept from shallower zones by currents and waves related to storms, that is, the 'wave-base razor' effect of Sonnenfeld & Cross (1993). Grainy sediments transferred down the slope were supplied by oligophotic (red algae, large foraminifers) and photo-independent (crinoids) biota of the middle ramp or outer shelf and upper slope of the clinoforms. Consistently, water depths for the upper clinoform slope parts, inferred from geometric restorations, range from 20 m (restricted basin for the Miocene, Turkey) (Janson *et al.* unpub. data) to 60 m (Permian, Last Chance Canyon, USA: Kerans, Jerry-Lucia & Senger, 1994). The general architecture and composition of clinoforms (progradation character of clinobeds which pinch out basinwards) reflect the outwards dispersal of carbonate sediment. Dispersal of material decreases as water depth and distance from source both increase. In such a depositional context, clinoform shape and slope angle of clinoforms are unlikely to reflect any hydrodynamic equilibrium profile but rather depend on the amount and nature (size) of the carbonate sediment recruited from the shelf or middle ramp by each storm event. Clinoform accretion is interpreted to result from intermittent transport of sediments along the slope due to recurrent storm events that affected the shelf or ramp. Each clinobed represents a single depositional event and such an episodic mode of sedimentation accounts for the nil to gradual facies change along clinobeds as well as possible pronounced vertical facies differentiation through clinobeds, as has been shown in Oman.

6. Conclusions

Shallow-water clinoforms from several ancient carbonate platforms exhibit great variability, with a complex combination of morphological and compositional attributes. Clinoforms range from exponential to oblique, with a dominant asymmetrical sigmoidal form. Maximum slope angles range from a few degrees to 25°, with the most common occurrence between 10 and 18°. Facies distribution along clinoforms shows well-defined zonation, or gradual passages, or near uniformity. Our study also reveals that there is no clear association between different attributes, such as shape versus slope, slope versus sediment fabric, slope versus relief.

Our results show that the environmental setting of clinoform progradation controls morphology. Proximal/shallow clinoforms display round-edged exponential profiles, and changes in sediment fabrics and sedimentary structures along the clinoform, whereas vertical facies differentiation is limited. Distal clinoforms show more diversified profiles and are generally shorter and steeper than their proximal counterparts. Facies differentiation is weak laterally, but may be very pronounced through the clinoforms.

As to the fundamental control of clinoform development across carbonate platforms, it is suggested that low-relief forms of proximal/shallow clinoforms, which contain coarse-grained and photo-independently produced debris, record hydrodynamic equilibrium profiles, whereas higher-relief forms on proximal/shallow clinoforms rather reflect a high differential production rate of carbonate sediment with water depth, secondarily smoothed by hydrodynamics. In distal settings, the carbonate bulk of clinobeds mainly derives from skeletal production by oligophotic and photo-independent biota of the middle ramp or outer shelf and upper portion of the clinoforms. The contribution by *in situ* skeletal biota only becomes significant on the lower slope. This means that distal slopes on carbonate shelves are not organically but hydrodynamically generated, even if the differentiation of these slopes may have subsequently induced the development of particular benthic forms (e.g. alveolinids in the Miocene).

Acknowledgements. This work was supported by the Institut National des Sciences de l'Univers through the programme 'Intérieur de la Terre', 'Comportement dynamique des systèmes sédimentaires carbonatés', and by the COPREP project 'Applications Pétrolières de la Stratigraphie Séquentielle'. We were shown field sights by J. Grotzinger in Namibia, J.-P. Garcia in Burgundy, K. J. McDonough in Vercors, J. Philip in Oman, F. Van Buchem and A.-M. Schwab in Turkey. Specific gratitude is due to P. W. Homewood for the invitation to participate in the COPREP Projects in Oman and Turkey, to T. Cross, J. Grotzinger and A.-M. Schwab for scientific discussion and to J. Kenter for an initial review. Thanks to C. Chateau-Smith for proofreading the English. The manuscript has benefited from constructive comments and remarks from W. Ahr and E. Adams.

References

ADAMS, E. W. & SCHLAGER, W. 2000. Basic types of slope curvature. *Journal of Sedimentary Research* **70**(4), 814–28.

ADAMS, E. W. & SCHLAGER, W. 2001. Morphology and curvature of delta slopes in Swiss lakes: lessons for the interpretation of clinoforms in seismic data. *Sedimentology* **48**(3), 661–79.

ADAMS, E. W., MORSILLI, M., SCHLAGER, W., KEIM, L. & VAN HOEK, T. 2002. Quantifying the geometry and sediment fabric of linear slopes: examples from the Tertiary of Italy (Southern Alps and Gargano Promontory). *Sedimentary Geology* **154**, 11–30.

ARNAUD, H. 1981. De la plate-forme urgonienne au bassin Vocontien: le Barrémo-Bédoulien des Alpes occidentales entre Isère et Buëch (Vercors méridional, Diois oriental et Dévoluy). *Mémoire Géologie Alpine* **3**, 804 pp.

BAHAMONDE, J., COLMENERO, J. & VERA, C. 1997. Growth and demise of late Carboniferous carbonate platforms in the eastern Cantabrian zone, Asturias, northwestern Spain. *Sedimentary Geology* **116**, 99–122.

BAHAMONDE, J., KENTER, J. A. M., DELLA PORTA, G., KEIM, L., IMMENHAUSER, A. & REIJMER, J. J. G. 2004. Lithofacies and depositional processes on a high, steep-margined Carboniferous (Bashkirian–Moscovian) carbonate platform slope, sierra del Cuera, NW Spain. *Sedimentary Geology* **166**(1–2), 145–56.

BIZON, G., BIJU-DUVAL, B., LETOUZEY, J., MONOD, O., POISSON, A., OZER, B. & OZTUMER, E. 1974. Nouvelles précisions stratigraphiques concernant les bassins tertiaires du sud de la Turquie (Antalya, Mut, Adana). *Revue de l'Institut français du Pétrole* **XXXIX 3**, 305–25.

BLENDINGER, W. 1994. The carbonate factory of Middle Triassic buildups in the Dolomites, Italy: a quantitative analysis. *Sedimentology* **41**, 1147–59.

BOSELLINI, A. 1984. Progradation geometries of carbonate platforms: examples from the Triassic of the Dolomites, northern Italy. *Sedimentology* **31**, 1–24.

CORSO, W., AUSTIN, J. A. & BUFFLER, R. T. 1989. The early Cretaceous platform off northwest Florida: controls on morphologic development of carbonate margins. *Marine Geology* **86**, 1–14.

DURLET, C. & THIERRY, J. 2000. Modalités séquentielles de la transgression aaléno-bajocienne sur le sud-est du Bassin parisien. *Bulletin de la Société Géologique de France* **171**, 327–39.

EBERLI, G. P., BERNOULLI, D., SANDERS, D. & VECSEI, A. 1993. From aggradation to progradation: the Maiella platform (Abruzzi, Italy). In *Cretaceous Carbonate Platforms* (eds A. Simo, R. Scott and J.-P. Masse), pp. 563–77. American Association of Petroleum Geologists, Memoir no. 56.

EVERTS, A. J. W., STAFLEU, J., SCHLAGER, W., FOUKE, B. & ZWART, E. W. 1995. Stratal Patterns, Sediment Composition, and Sequence Stratigraphy at the Margin of the Vercors Carbonate Platform (Lower Cretaceous, SE France). *Journal of Sedimentary Research* **B65**, 119–31.

GERMS, G. J. B. 1983. Implications of a sedimentary facies and depositional environmental analysis of the Nama group in south west Africa/Namibia. *Special Publication of the Geological Society of Africa* **11**, 89–114.

GRACIANSKY, P. & LEMOINE, M. 1988. Early Cretaceous extensional tectonics in southwestern French Alps: a consequence of North Atlantic rifting during Tethyan spreading. *Bulletin de la Société Géologique de France* **8**, 733–7.

GROTZINGER, J. P., BOWRING, S. A., SAYLOR, B. Z. & KAUFMAN, A. J. 1995. Biostratigraphic and geochronologic constraints on early animal evolution. *Science* **270**, 598–604.

GUILLOCHEAU, F., ROBIN, C., ALLEMAND, P., BOURQUIN, S., BRAULT, N., DROMART, G., FRIEDENBERG, R., GARCIA, J., GAULIER, J., GAUMET, F., GROSDOY, B. & HANOT, F. 2000. Meso-Cenozoic geodynamic evolution of the Paris Basin: 3D stratigraphic constraints. *Geodinamica Acta* **13**, 189–246.

HARRIS, M. 1994. The foreslope and toe-of-slope facies of the Middle Triassic, Latemar buildup (Dolomites, northern Italy). *Journal of Sedimentary Research* **B64**, 132–45.

HOTTINGER, L. 1997. Shallow benthic foraminiferal assemblages as signals for depth of their deposition and their limitations. *Bulletin de la Société Géologique de France* **168**, 491–505.

JACQUIN, T., ARNAUD-VANNEAU, A., ARNAUD, H., RAVENNE, C. & VAIL, P. 1991. Systems tracts and depositional sequences in a carbonate setting, a study of continuous outcrops from platform to basin at the scale of seismic lines. *Marine Petroleum Geology* **8**, 122–39.

KEIM, L. & SCHLAGER, W. 1999. Automicrite facies on steep slopes (Triassic, Dolomites, Italy). *Facies* **41**, 15–26.

KENTER, J. A. M. 1990. Carbonate platforms flanks: slope angle and sediment fabric. *Sedimentology* **37**, 777–94.

KENTER, J. A. M. & CAMPBELL, A. 1991. Sedimentation on a Lower Jurassic carbonate platform flank: geometry, sediment fabric and related depositional structures (Djebel Bou Dahar, High Atlas, Morocco). *Sedimentary Geology* **72**, 1–34.

KERANS, C., JERRY LUCIA, F. & SENGER, R. K. 1994. Integrated Characterization of Carbonate Ramp Reservoirs Using Permian San Andres Formation Analogs. *American Association of Petroleum Geologists Bulletin* **78**, 181–216.

MASSE, J., BELLION, Y., BENKHELIL, J., RICOU, L., DERCOURT, J. & GUIRAUD, R. 1993. Early Aptian. In *Atlas Tethys palaeoenvironmental Maps* (eds J. Dercourt, L. Ricou and B. Vrielynck), pp. 135–52. Explanatory notes. Gauthier-Villars: Paris.

MITCHUM, R., VAIL, P. & SANGREE, J. 1977. Seismic stratigraphy and global changes of sea level, Part 6. stratigraphic interpretation of seismic reflection patterns in depositional sequences. In *Seismic Stratigraphy, Applications to Hydrocarbon Exploration* (ed. C. Payton), pp. 117–33. American Association of Petroleum Geologists, Memoir no. 26.

MULLINS, H., HEATH, K. C., VAN BUREN, H. M. & NEWTON, C. R. 1983. Anatomy of a modern open-ocean carbonate slope: northern Little Bahamas Bank. *Sedimentology* **31**, 141–68.

PHILIP, J., BORGAMANO, J. & AL-MASKIRY, S. 1995. Cenomanian–Early Turonian carbonate platform of northern Oman: stratigraphy and palaeo-environments. *Palaeogeography, Palaeoclimalology, Palaeoecology* **119**, 77–92.

POMAR, L. 1991. Reef geometries, erosion surfaces and high-frequency sea-level changes, Upper Miocene reef complex, Mallorca, Spain. *Sedimentology* **38**, 243–69.

POMAR, L., OBRADOR, A. & WESTPHAL, H. 2002. Subwavebase cross-bedded grainstones on a distally-steepened carbonate ramp, Upper Miocene, Menorca, Spain. *Sedimentology* **49**, 139–69.

QUIQUEREZ, A., ALLEMAND, P., DROMART, G. & GARCIA, J.-P. 2004. Impact of storms on mixed carbonate and silicilastic shelves: insights from combined diffusive and fluid-flow transport stratigraphic forward model. *Basin Research* **16**, 431–49.

READ, J. F. 1985. Carbonate platform facies models. *American Association of Petroleum Geologists Bulletin* **69**(1), 1–21.

RICH, J. L. 1951. Three critical environments of deposition, and criteria for recognition of rocks deposited in each of them. *Geological Society of America Bulletin* **62**, 1–20.

ROBIN, C., GUILLOCHEAU, F., ALLEMAND, P., BOURQUIN, S., DROMART, G., GAULIER, J.-M. & PRIJAC, C. 2000. Echelles de temps et d'espace du contrôle tectonique d'un bassin flexural intracratonique: le bassin de Paris. *Bulletin de la Société Géologique de France* **171**, 181–96.

ROUSSELLE, B. & DROMART, G. 1996. Partition stratigraphique des environnements et produits carbonatés dans l'Aalénien du sud-est de la France. *Bulletin de la Société Géologique de France* **167**, 399–408.

SAYLOR, B., KAUFMAN, A., GROTZINGER, J. & URBAN, F. 1998. A composite reference section for Terminal Proterozoic strata of southern Namibia. *Journal of Sedimentary Research* **68**, 1223–35.

SCHLAGER, W. & CAMBER, O. 1986. Submarine slope angles, drowning unconformities, and shelf-erosion on limestone escarpments. *Geology* **14**, 762–5.

SONNENFELD, M. 1991. High Cyclicity within Shelf-Margin and Slope Strata of the upper San Andres Sequence, Last Chance Canyon. In *Sequence Stratigraphy, Facies, and Reservoir Geometries of the San Andres, Grayburg, and Queen Formations, Guadalupe Mountains, New Mexico and Texas, Permian Basin Section* (eds S. Meader-Roberts, M. P. Candelaria and G. E. Moore), pp. 11–52. SEPM Annual Field Trip, Publication no. 91-32.

SONNENFELD, M. & CROSS, T. 1993. Volumetric partioning and facies differentiation within the Permian upper San Andres Formation of Last Chance Canyon, Guadalupe Mountains, New Mexico. In *Recent advances and applications of carbonate sequence stratigraphy* (ed. R. Loucks), pp. 435–74. American Association of Petroleum Geologists, Memoir no. 29.

SWIFT, D. J. P. & THORNE, J. A. 1991. Sedimentation on continental margins. In *shelf sand and sandstone bodies* (eds D. J. P. Swift, G. F. Oertel, R. W. Tillman and J. A. Thorne), pp. 3–31. International Association of Sedimentologists, Special Publication no. 14.

VAN BUCHEM, F. S. P., RAZIN, P., HOMEWOOD, P., OTERDOOM, W. H. & PHILIP, J. 2002. Stratigraphic organization of carbonate shelves and organic-rich intrashelf basins: Natih Formation (Middle Cretaceous) of northern Oman. *American Association of Petroleum Geologists Bulletin* **86**, 21–53.

VECSEI, A. 1998. Bioclastic sediment lobes on a supply dominated Upper Cretaceous carbonate platform margin, Montagna della Maiella, Italy. *Sedimentology* **45**, 473–87.

WEBER, L. J., KERANS, C. & NANCE, H. S. 1991. Road Log: Second Day Carlsbad, New Mexico to Algerita Escarpment via Dark Canyon. In *Sequence Stratigraphy, Facies, and Reservoir Geometries of the San Andres, Grayburg, and Queen Formations, Guadalupe Mountains, New Mexico and Texas, Permian Basin Section* (eds S. Meader-Roberts, M. P. Candelaria and G. E. Moore), pp. 71–90. SEPM Annual Field Trip Publication no. 91-32.

WILLIAMS, G., ULUGENC, U., KELLING, G. & DEMIRKOOL, C. 1995. Tectonic control on stratigraphic evolution of the Adana basin, Turkey. *Journal of the Geological Society, London* **152**, 873–82.